THE POLARIZATION OF THE RECOIL PROTON IN ETA PHOTOPRODUCTION

Thesis by

Bruce D. Winstein

In Partial Fulfillment of the Requirements

For the Degree of

Doctor of Philosophy

California Institute of Technology

Pasadena, California

1970

(Submitted May 21, 1970)

ACKNOWLEDGMENTS

Thank you, Clemens Heusch, for your guidance, advice and high standards of excellence throughout the whole course of the experiment and my stay at Caltech.

Thank you, Charles Prescott, for your concern. To you I am also indebted for your having designed much of the equipment which I used in my experiment.

Thank you, Leon Rochester, for your daily interest in my problems with the analysis of the experiment. I here acknowledge your considerable work, both conceptual and in the form of computer programs, which I took over for my own analysis.

Thank you, Walter Nilsson, for constructing much of the equipment which I used, and for the active part you played in the setting up of the experiment.

I say thanks to the other members of the group, who helped in many ways besides the running of the experiment; in particular, to Bill McNeely and to Kirk McDonald.

Thank you, Phyllis Nilsson, for your programming help, and general encouragement.

The Synchrotron crew, under the direction of Paul Van Ligten, and the synchrotron operators, headed by Al Neubieser, kept the synchrotron in operation without breakdown during the running of my experiment. To all of you I am grateful.

My thanks go to Earle Emery, Dick Wileman and Bill Friedler for their active assistance.

To all of my scanners, under the direction of Sherwood Wilner and Michael Carter, I say thank you for your careful work.

Thank you, Kathy Barlow, for your work beyond the call of duty in the typing of my thesis.

For financial support, I am indebted to the NDEA, to the California Institute of Technology, and to the State of California.

Thank you, Mr. Layton, for giving me such an inspired and enthusiastic first exposure to physics.

ABSTRACT

We measured the recoil proton polarization in the process $\gamma p \to p\eta$ at the 1.5 GeV Caltech electron synchrotron, at photon energies from 0.8 to 1.1 GeV, and at center-of-mass production angles around 90°. A counter-spark chamber array was used to determine the kinematics of all particles in the final state of the partial mode $\gamma p \to p\eta$ $(\eta \to 2\gamma)$. The protons' polarization was determined by measuring an asymmetry in scattering off carbon. Analysis of 280,000 pictures yielded 2400 useful scatters with a background which was 30% of the foreground. The polarization results show a sizeable opposite parity interference at 830 MeV, 950 MeV, and 1100 MeV.

TABLE OF CONTENTS

LIST OF FIGURES

LIST OF FIGURES (cont.)

LIST OF FIGURES (cont.)

LIST OF TABLES

To my family

Work of sight is done,
now do heart-work
on the pictures within you, those captives; for you
overcame them: but now do not know them.
Behold, inner man, your inner maiden,
this, won from
a thousand natures, this
creature, now only won,
never yet loved.

--Rainer Marie Rilke

I. INTRODUCTION

In this experiment, we measure the polarization of the recoil proton in the reaction

$$\gamma + p \rightarrow p + \eta$$

for center-of-mass production angles around 90° and at photon energies from 0.8 to 1.1 MeV.

Figure 1.1 shows all the information known about eta photoproduction before we first fired our spark chambers. The figure shows a large peak immediately above threshold which is close to isotropic in angular distribution; this feature of the eta photoproduction cross-section is most likely explained by the presence of the nucleon isobar $S_{11}(1550)$ as an intermediate state.

New data on eta photoproduction from Daresbury[23] show a distinct second peak at a mass value of about 1760 MeV. It is believed that this peak is due to the presence of the isobar $P_{11}(1750)$. Indeed, with this isobar and the established $S_{11}(1550)$, all the features of figure 1.1 and the new data are well fitted,[1,24] including the dip in the region around 1650 MeV and the flat peak around 1700-1800 MeV. We note, however, that only very few data exist, so that the few constraints they yield make a model incorporating only few terms a satisfactory fit.

At comparable energies in pion photoproduction, however, the situation is more complicated. Many isobars can and do contribute; as a result, angular distributions are complicated and as well, the polariza-

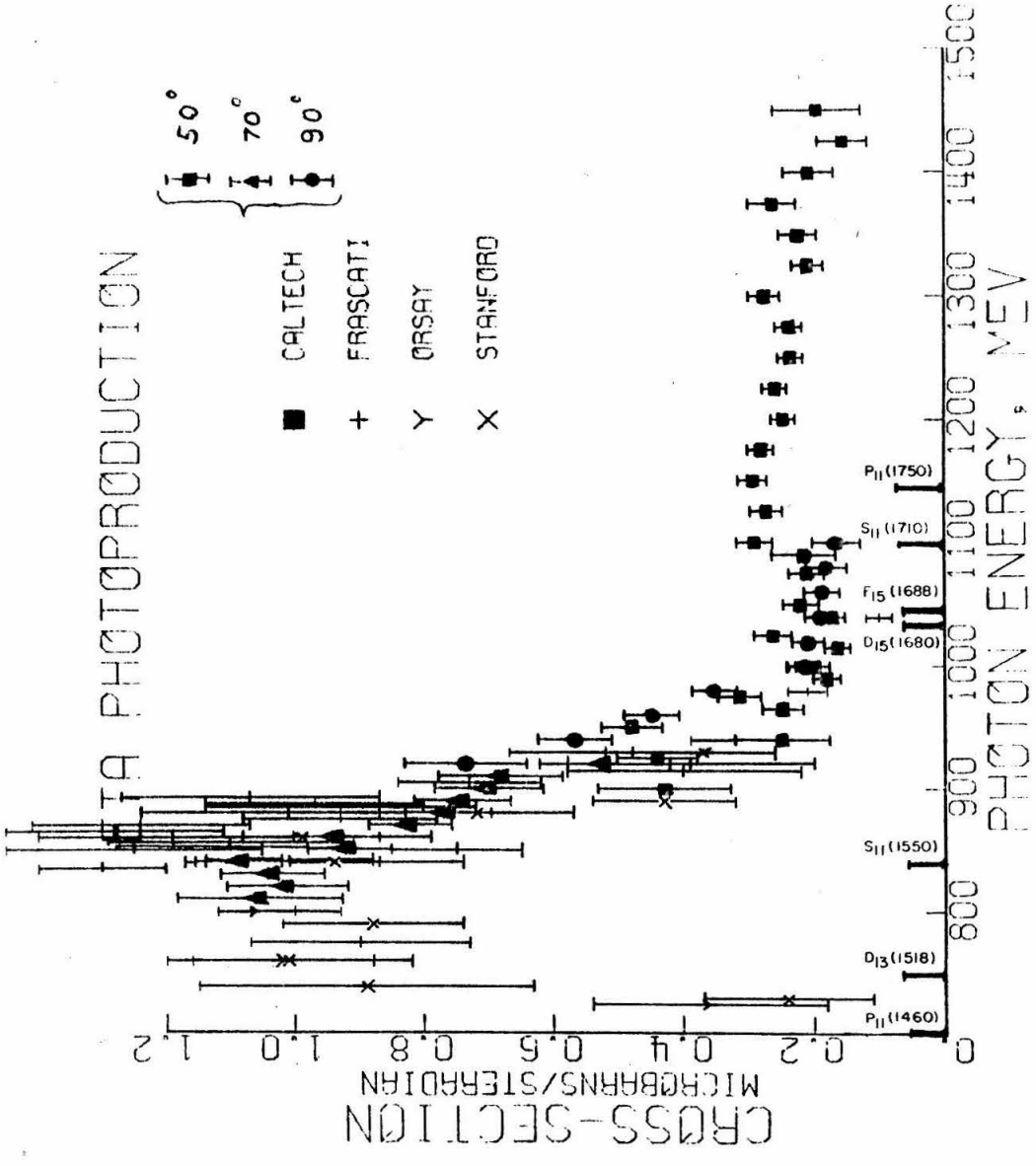

Figure 1.1 Eta photoproduction cross-section.

tion has a steep angular dependence.[2,3,4]

In eta photoproduction, only the $I = \frac{1}{2}$ channel contributes and therefore fewer isobars are expected. As a result, the cross-section and its angular distribution exhibit much simpler features than in the case of pion photoproduction.

We note from figure 1.1 that two $I = \frac{1}{2}$ resonances which are prominent in pion photoproduction, the $D_{13}(1512)$ and the $F_{15}(1688)$, do not appear to contribute in the photoproduction of the eta meson. The $D_{13}(1512)$ is close to threshold and therefore suppressed by an angular momentum factor $q^{2\ell + 1} = q^5$ (q is the center-of-mass momentum). The $F_{15}(1688)$ does not show up because of SU(3) Clebsch-Gordon coefficients.[5]

The isobars known from πp scattering which do contribute to $\gamma p \to p\eta$ all have $J = \frac{1}{2}$, and the question of their photoexcitability has interesting consequences with respect to symmetry and quark model considerations.

As an example, we consider the states $D_{15}(1680)$ and $S_{11}(1710)$. These are not required in phenomenological fits. Moorhouse[6] has pointed out that the quark model predicts that these resonances cannot be photoexcited. Yet the $S_{11}(1710)$ resonance <u>could</u> be photoexcited even in that model, but only if there is mixing between it and the $S_{11}(1550)$.[7]

Another interesting question is whether the $P_{11}(1460)$, the "Roper resonance", can be photoexcited. This resonance, with the same quantum

numbers as the nucleon, was first identified in pion-nucleon phase shift analysis by Roper et al.[8] A peak at the right mass value has been observed in small-angle p-p and π-p inelastic scattering at several energies.[9, 10, 11] However, analyses of both the pion and eta photoproduction angular distributions do not require a $P_{11}(1460)$ contribution. This is not surprising, however, because the $P_{11}(1460)$, were it present, would appear under the peak of the $D_{13}(1512)$ and would as well be under the tail of the $P_{33}(1238)$, in pion photoproduction. In eta photoproduction, unless it were strongly produced, the $P_{11}(1460)$ would be hard to identify in the presence of the $S_{11}(1550)$, without better angular distributions than are presently known.

If the $P_{11}(1460)$ can be photoexcited off neutrons but not protons (i.e., the vertex $\gamma p N^*(1460)$ vanishes but $\gamma n N^*(1460)$ does not), then U-spin conservation implies that it belongs to a $\overline{10}$ in SU(3). Thus information on the photoexcitability of the $P_{11}(1460)$ can help to establish its SU(3) assignment, which is not yet certain.

How then can we find out about these weaker states, namely the $P_{11}(1460)$ and $S_{11}(1710)$, if the $S_{11}(1550)$ and $P_{11}(1750)$ dominate the mechanism? The states in which we are interested each occur in a region where the dominating state has opposite parity; therefore the answer is to perform an experiment which is sensitive to interference terms that arise between opposite parity states.

We are doing a high statistics experiment on the 0° - 180° asymmetry in eta photoproduction near threshold which should be sensitive to the presence of any P wave admixture.[12]

Photoproduction experiments with polarized photons or a polarized target are also sensitive to opposite parity interference and will no doubt be done after technical advances make them more feasible. The recoil proton polarization is also sensitive to opposite parity interference; in fact it was by such an experiment that the relative parity of the first and second resonances was established.

We performed our recoil proton polarization experiment at 90° to yield information on $P_{11}(1460)$ as well as $S_{11}(1710)$. The $P_{11}(1460)$ lies below threshold in the ηp channel, but because it is very broad, its tail may contribute. If so, its interference with the $S_{11}(1550)$ could show up prominently in a polarization experiment at 90°.

Similarly, a sizeable polarization at 90° in the region of the $P_{11}(1750)$ could indicate an interference with the $S_{11}(1710)$; the presence of the latter would lead us to the conclusion that there is $S_{11}(1710) - S_{11}(1550)$ mixing.

Thus we chose our kinematical region to be sensitive to opposite parity interference in the region spanned by the $S_{11}(1550)$ and the $P_{11}(1750)$. In photon energy, this region corresponds to from 800 to 1150 MeV. Recoil proton energies at these k values range from 100 to 300 MeV. This is convenient for using carbon as a polarization analyzer: the analyzing power of carbon is both well known and sizeable in this region of proton energies.

We will see in Section IV that our results do indeed indicate the presence of S-P interference at both regions of interest.

II. EXPERIMENTAL METHOD

We wished, then, in this experiment to study the recoil proton polarization in the reaction

$$\gamma + p \rightarrow p + \eta$$

at energies from 0.8 to 1.1 GeV. Our experimental group had previously described the methods, described below, necessary to identify the above reaction; the contribution of the present experiment in this respect was to run in such a configuration that our detection efficiency was about fifteen times that of our previous cross-section experiment.[13] In spite of the fact that this meant an inevitable loss in experimental resolution, the increase in detection efficiency was necessary. The protons' polarization was determined by an asymmetry in scattering off carbon, which is the most useful element to use for a polarization determination from protons in the energy range of the present experiment (90 - 280 MeV). Nevertheless, because of the size of the p-C scattering cross-section, only 3-4% of our fully identified events could be used in such an analysis.

The general experimental area is shown in figure 2.1 with the apparatus particular to the present experiment shown schematically in figure 2.2. Circulating electrons at energy E_o strike a tantalum target and produce the photon bremsstrahlung beam. The Caltech synchrotron produced a uniform photon beam for about 170 milliseconds during each one-second acceleration cycle. The emerging beam was collimated and swept before passing through the hydrogen target and finally stopped and

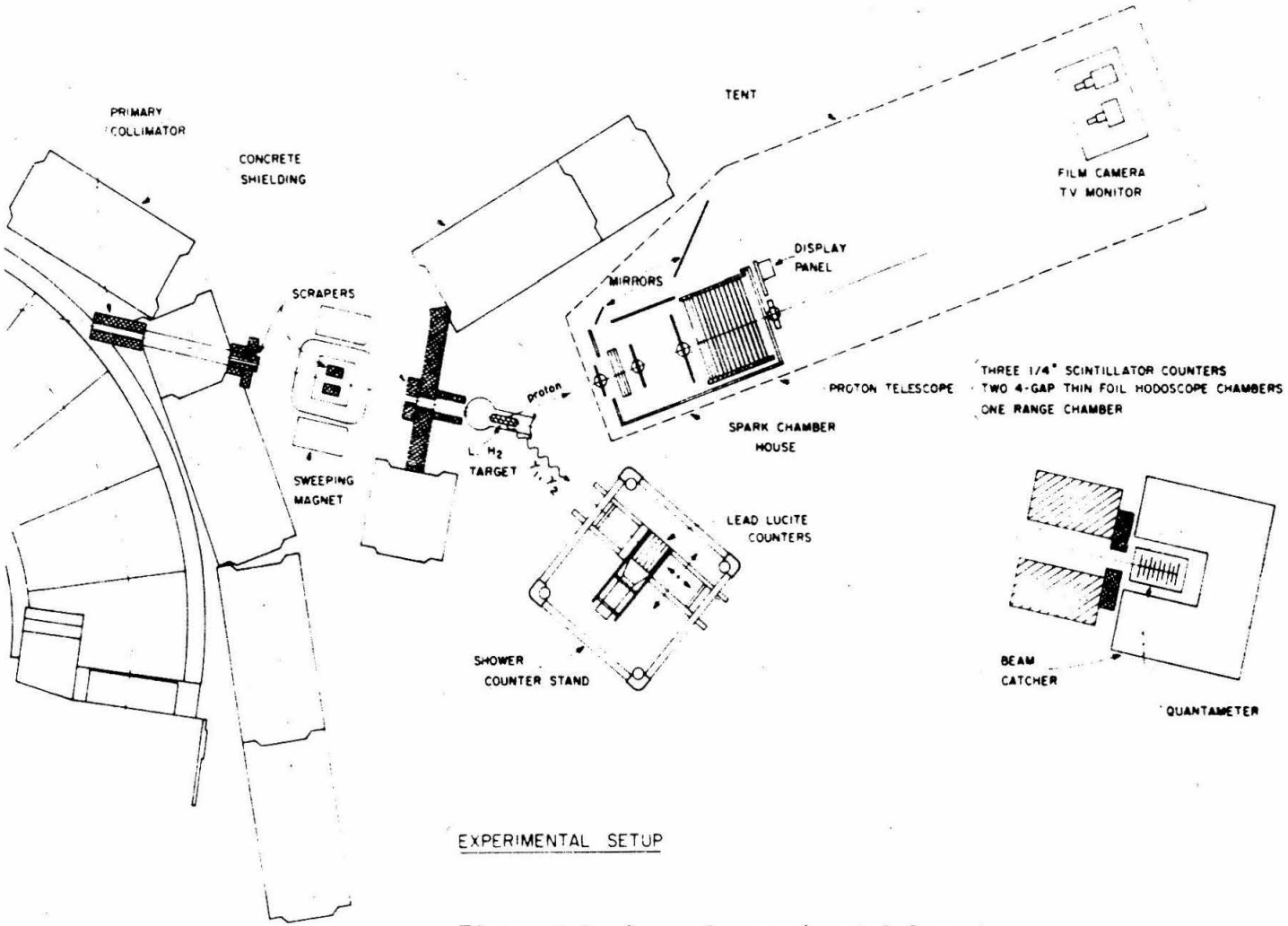

Figure 2.1 General experimental layout

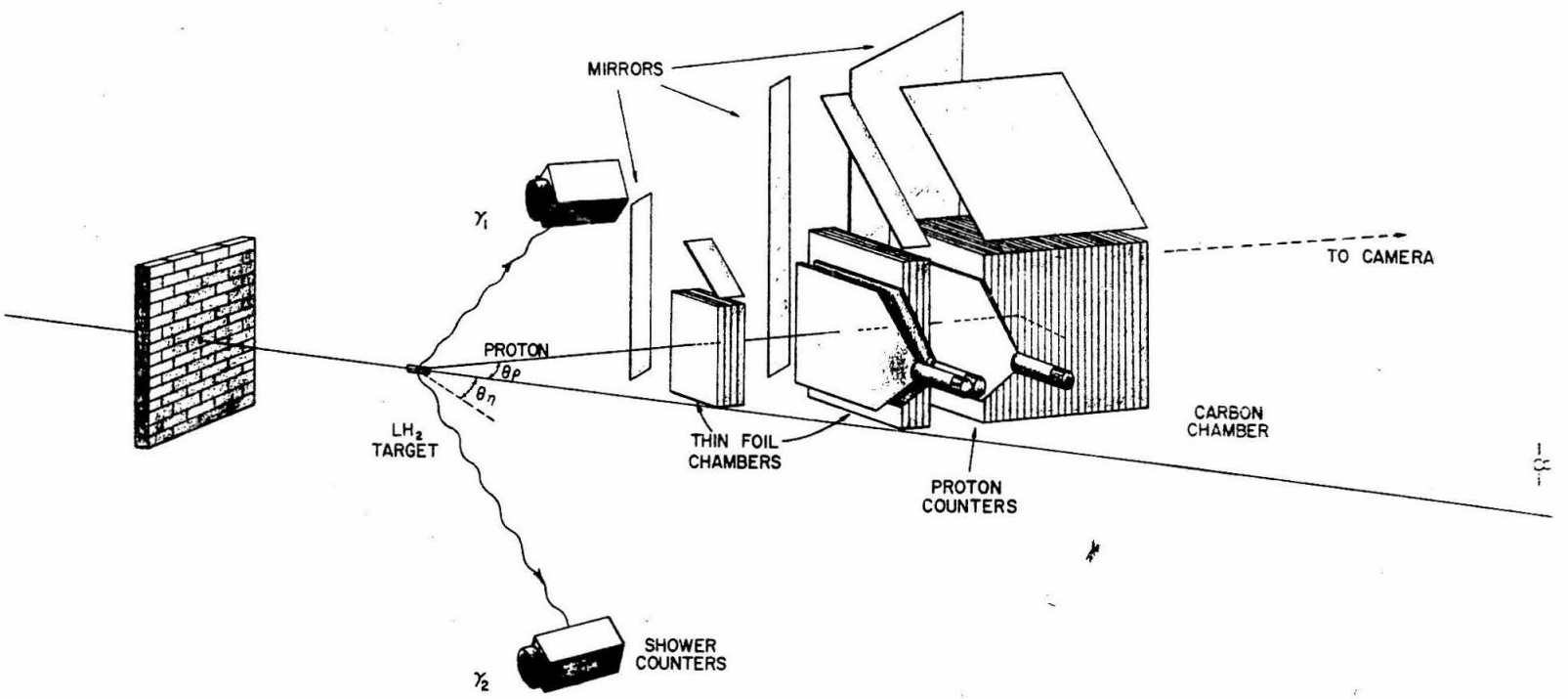
MIRRORS
γ_1
PROTON
θ_p
θ_η
LH_2
TARGET
THIN FOIL
CHAMBERS
PROTON
COUNTERS
CARBON
CHAMBER
TO CAMERA
SHOWER
COUNTERS
γ_2
EXPERIMENTAL SETUP

Figure 2.2

monitored in a quantameter. (The photon beam is described in more detail in Appendix VI-1, the hydrogen target in Appendix VI-2.)

The recoil proton from $\gamma p \rightarrow p\eta$ was detected by means of a proton telescope consisting of three scintillation counters and three optical spark chambers. (See figure 2.2). A proton was defined by a triple-coincidence among the scintillation counters whose biases had been adjusted for maximum proton efficiency and minimum electron or pion efficiency. (See Appendix VI-4). The first two spark chambers defined the proton direction while the third chamber, consisting of spark-chamber modules alternating with carbon plates, served as a scattering chamber while also yielding information on the proton energy from its range in the carbon. The (known) direction of the incident photon and the direction of the proton defined for us the reaction plane.

The eta was identified by simultaneous detection of both gammas from its 41% decay mode, $\eta \rightarrow 2\gamma$. Two gamma detection systems were set up on the opposite side of the beam from the proton telescope, the plane formed by the two being perpendicular to the (average) reaction plane. The angle that the intersection of these two planes made with the incoming photon beam was the central eta angle and was determined from kinematics. The two detection systems were placed symmetrically above and below the reaction plane; thus we were looking at etas whose decay photons, on the average, come off symmetrically with respect to the eta direction: this procedure yields the largest detection efficiency for $\eta \rightarrow 2\gamma$.

Each photon detection system consisted of ¼" lucite (to shield from very soft electrons), a veto scintillation counter, two radiation lengths of lead to convert the gamma, a 4 x 5 system of overlapping crossed hodoscope counters, and a lead lucite shower counter. This system is described in detail in Appendix VI-3. A "gamma" signal was defined by a simultaneous signal from at least one vertical and one horizontal hodoscope counter and a sufficiently high pulse height in the shower counter, in the absence of a veto signal.

A three way coincidence between the two photon systems and the proton telescope indicated a possible event and defined our trigger. When the logic indicated such a coincidence, we fired our spark chambers; this made the proton track visible to a camera which photographed the chambers both from the side and from the top by a system of mirrors. Fiducial marks were illuminated, 15 for each of the two views of the chambers, and photographed on the same frame of film; in this way we could determine the location of sparks in the lab. Also photographed on the same frame of film was a panel of lights which were flashed to indicate the particular hodoscope counters which participated in each photon shower, as well as the pulse-heights in each shower counter. The film was then advanced; we were able to record just one trigger per synchrotron pulse--on the average the trigger rate was one per 15 synchrotron pulses. In this manner, information was collected for about 280,000 triggers in about 1500 hours of running at two kinematical settings. Table 2.1 summarizes the parameters of each setting and shows the amount of data collected at each.

Table 2.1

KINEMATICAL PARAMETERS

SETUP	$\langle k \rangle$ MeV	$\langle \theta_\eta^* \rangle$ deg	θ_p° deg	θ_η° deg	$\theta_{\gamma\gamma}^\circ /2$ deg	T_p MeV	E_η MeV	E_o MeV	Triggers
I	850	90	25.48	37.53	53.13	165	685	980	200,000
II	1050	80	34.80	37.62	41.07	216	834	1150	80,000

For each setting, $\langle k \rangle$ and $\langle \theta_\eta^* \rangle$ are the nominal photon energy and center of mass production angle. θ_p°, θ_η°, $\theta_{\gamma\gamma}^\circ$ are central values of the laboratory proton angle, eta angle and $\eta \rightarrow 2\gamma$ opening angle. T_p is the average proton kinetic energy; E_η the average eta total energy. E_o is the end point energy of the synchrotron.

Figure 2.3 Two typical event pictures (shown in negative).

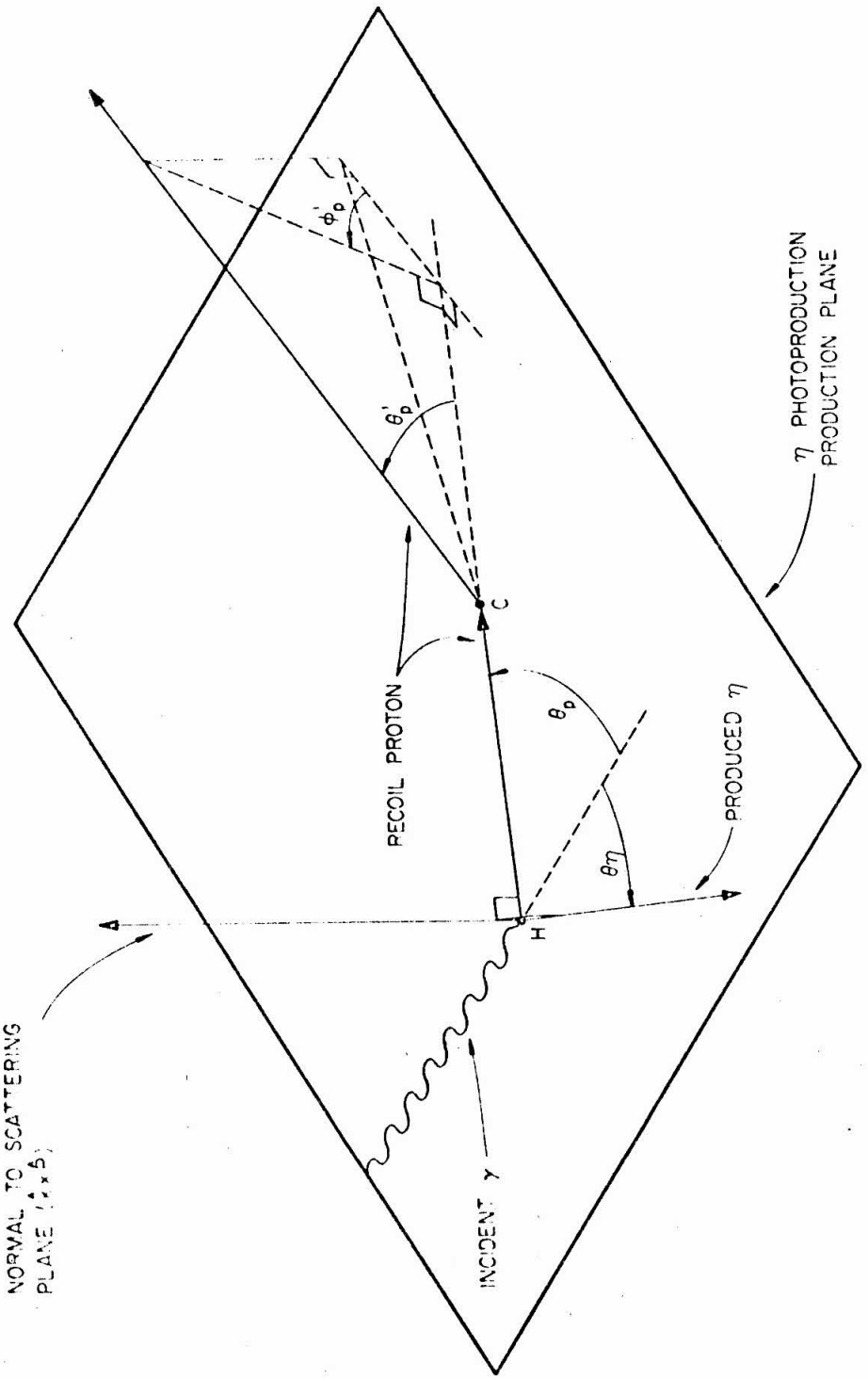

Figure 2.4 γp and p-C interaction diagram.

All the primary data for each event appeared on one frame of 35 mm film; two typical frames are shown in figure 2.3. The event on the right of the figure shows a proton scatter, the one on the left does not. In addition, for each run (750 triggers), rates were recorded for all important counters in the experiment as well as for coincidences at all levels in the logic. In this way dying phototubes and dead transistors were quickly noticed (and buried).

Figure 2.4 shows schematically the relationship between the initial reaction plane, $\gamma p \rightarrow p\eta$, and the proton-carbon scattering plane. On the average the top view of the events in figure 2.3 shows the projection of the p-C scatter onto the initial reaction plane.

Let us see how the information collected can be used in the reconstruction of the event. There are five particles present ($\gamma p \rightarrow p\gamma\gamma$), each of which has four quantities to be determined, yielding a total of 20 numbers to determine. Conservation of energy-momentum gives us four relations, the known masses of the photons yield three more relations. In addition the known direction of the incoming photon as well as the measured directions of the two final state photons give us six more known quantities. Also, we know the mass of the initial proton and that it is at rest: four more quantities. Finally, we measure the direction and energy, (if we assume for the moment that we have an elastic p-C scatter), of the final state proton, which yields its 4-momentum. We then have determined 21 relations among 20 unknowns. We will see in the next section how we were able to effectively exclude most of our background with this one parameter over-determination in spite of our inability to resolve the p-C inelasticity.

III. DATA ANALYSIS

In this section we will discuss the various criteria by which our 280,000 pictures were reduced to roughly 2400 "useful" "foreground" events as well as the analysis of these "useful" events leading to a polarization determination at 5 photon energies and at center-of-mass production angles around 90°.

1. Scanning and Measuring

The major cut occurred in the scanning and measuring stage of the experiment, about 18,000 triggers surviving. Scanning and measuring will be treated more fully in Appendix VI-6; the scanners were instructed to record and measure any event where it appeared that (a) one photon each went into the photon telescopes (see Appendix VI-3 for further details), (b) where the associated proton underwent a clear scatter of at least 3°, and (c), where at least 2 carbon plates existed between the scattering vertex and the stopping point of the proton. The number 3° was chosen with the idea that in the final analysis, only scatters with angles on the scanning table greater than 4° would be used: with any cutoff one chooses, it is very hard to get an unbiased selection near the cutoff angle itself. We will see later that because of the size of the carbon analyzing power for scatters less than 4°, this region contributes very little anyway to a polarization determination.

The requirement of two modules of carbon between the vertex and the stopping point was imposed for two reasons: (1) 2 carbon modules corresponded on the average to about 75 MeV and at energies below this

number, the carbon analyzing power is small and not well known; and (2), to make an accurate measurement on the proton track after the scatter, at least 3 sparking modules were required (there were 2 sparking modules between each pair of carbon plates).

Most of the 280,000 frames had 2-photon signatures (≈80%) so that this cut on the scanning table down to 18,000 pictures is pretty nearly a reflection of the size of the p-C scattering cross-section; most events simply did not scatter.

All the events which survived the cut on the scanning table were measured. This process consisted in digitizing all the information on the frame and punching this information on IBM cards. In particular, on the proton side x and y coordinates of the proton sparks in the two views of all three chambers, with the coordinates of 12 fiducial lights, were digitized for each event. On the photon side, the scintillation counters participating in the photon showers as well as the shower pulse-heights in the lead-lucite shower counters were digitized and recorded. All the IBM cards were directly transferred to one 2400 ft. magnetic tape. This tape was run through a major analysis program which generated another magnetic tape consisting of all calculated quantities for each event, there being 18,000 events at this stage. We will call this the preliminary analysis stage. This tape was then run through a program utilizing the maximum likelihood method to calculate the most likely proton polarization responsible for any left-right asymmetry in the p-C scatters, for any desired cut on the events.

The preliminary analysis stage will be described by discussing the cuts made on the data for one particular run through the maximum likelihood program.

Throughout this section, we will be referring to table 3.1 which shows how, for Setup 1, over 10,000 of 12,000 events were rejected.

2. Proton Reconstruction

Before the proton track could be reconstructed in the lab, it was necessary to locate the fiducials.

The coordinates of the measured fiducials were fit to a master grid by a transformation of the coordinate system which was constrained only to preserve straight lines. In this way, rotation and translation of the film in the frame holder, changes in film size due to temperature and humidity effects as well as misalignment of the mirrors in the projection system could be corrected. More fiducials were measured than there were parameters in the fit, so that a χ^2 for the fit was calculated. A large χ^2 would reflect a measuring error--35 events for this setting were rejected on the grounds of a poor grid fit.

As we mentioned before, the proton passed through two spark chambers, each chamber consisting of two two-gap modules, before entering the range chamber so that there were 8 sparks on the proton trajectory before any proton-Carbon scattering could occur. After being corrected by the coordinate transformation mentioned above, the 4 of these sparks that were measured were fitted to a line in three dimensions: table 3.1 shows that 18 events were rejected because of too large a

TABLE 3.1

SUMMARY OF REJECTED EVENTS, SET I, FOREGROUND

Criteria	# of Events
Grid Fit	35
Proton Trajectory	18
Target	414
L Type	1726
XMN1	4206
DELE	1587
IPH1	242
IPH2	288
ANGMAX	208
ANGMIN	752
TPFMAX	0
TPFMIN	1031
ANPMIN	25
PHOTON K	17
Total Number of Rejected Events	10549
Total Number of Events Processed	1793

χ^2--these events could have scattered in the scintillator between the two chambers.

Once the parameters of the proton trajectory were determined, the proton line was extrapolated back to the target to determine the event origin. The main uncertainty was due to the finite diameter of the target. The event origin was chosen on the midpoint of the intersection of the trajectory with the target. The trajectories of 414 of the events at the setting under discussion did not intersect the hydrogen target and were therefore rejected.

Table 3.1 next shows a cut of 1726 events. This large cut is a result of the fact that, in this experiment, we needed to know in which carbon module the proton stopped after scattering in order to accurately suppress backgrounds. An event was of this type if its track left the range chamber after scattering, or could have left without causing another gap to spark. We have seen in Section II that, assuming an elastic scatter, we are only one parameter overdetermined; for events which leave the chamber after scattering, we lose this overdetermination, and as we will see, suppression of backgrounds becomes impossible.

Also included in this cut was a small number of events which did not leave the chamber but were not used in the likelihood determination of the polarization for a reason described in Appendix VI-10F.

3. Kinematical Reconstruction

The proton direction (before the scatter) together with the known direction of the incoming γ-ray define the reaction plane. From the event origin and the hodoscope information, we determine the trajectories of the two decay photons of the η. The direction of the η itself is the intersection of the reaction plane with the plane of its two decay photons. It is now obvious why we placed our counters in such a way that these two planes were, on the average, perpendicular to each other: in this way we obtain the minimum uncertainty in the determination of the direction of the η. From the two angles, θ_1 and θ_2, that the decay photons make with respect to the η direction, we found the velocity of the η, β_η, from the following expression:

$$\beta_\eta = \frac{\sin(\theta_1 + \theta_2)}{\sin\theta_1 + \sin\theta_2}$$

Next, the proton energy was calculated, assuming an elastic p-C scatter, from its total range in the carbon plate chamber. The effects of a non-normal incidence, an off-center origin in the target and the carbon recoil energy were included where necessary. In practice, the proton kinetic energy, T_p, was calculated from the following expression:

$$\log T_p = \sum_{i=0}^{3} a_i \log R^i$$

where R is the total proton range, including the material in front of the range chamber, and the a_i's were determined by fitting the known range-energy data for carbon to the above expression. The expression

was good to within 0.3 MeV (of the tabulated values) for proton energies between 40 and 300 MeV. The experimental uncertainty in the proton energy, assuming an elastic p-C scatter, was about 6 MeV, resulting mainly from the finite size of the carbon plates. Of course, if the p-C scatter were highly inelastic, our determination of the proton energy from its range would be very inaccurate. For the distribution of proton energies involved in the present experiment, an inelasticity of ΔE gives rise to an under-estimate of the proton energy by an amount, on the average, of 0.8 ΔE. Because of the nature of the p-C scattering cross-section in the region of the present experiment, the majority of our protons did scatter elastically off the carbon. The effect of inelasticities, however, is not small and will be discussed in greater detail later.

The incoming photon energy, k, was calculated using the above determination of the proton energy together with the proton trajectory itself, from the following expression

$$k_1 = \frac{M_p E_p - M_p^2 + \mu^2/2}{M_p - E_p + p_p \cos\theta_p}$$

where M_p, E_p, p_p, θ_p are, respectively, the proton mass, energy, momentum, and lab production angle, and μ is the mass of the η, 549 MeV. Since in this expression we are also assuming that the two final state photons came from an eta, we are here <u>two</u> parameters overdetermined so that there are three different ways of calculating the photon energy. The other two ways, which do not assume an elastic p-C vertex, were

$$k_2 = \frac{M_p E_\eta - \mu^2/2}{M_p - E_\eta + p_\eta \cos\theta_\eta}$$

where θ_η is the η production angle in the lab, and E_η and p_η the eta energy and momentum calculated from the expression for β_η given above; and

$$k_3 = p_p(\cos\theta_p + \frac{\sin\theta_p}{\sin\theta_\eta} \cos\theta_\eta)$$

where p_p, the proton momentum is calculated from the conservation of energy relation:

$$p_p(\cos\theta_p + \frac{\sin\theta_p}{\sin\theta_\eta} \cos\theta_\eta) + M_p = \sqrt{p_p^2 + M^2} + \sqrt{p_p^2 \frac{\sin^2\theta_p}{\sin^2\theta_\eta} + \mu^2}.$$

In practice, a quartic equation was solved for p_p.

Next, the mass of the η meson itself was calculated in two independent ways, the first assuming an elastic p-C event, and the second not. The first expression is:

$$XMN1 = \left[(p_p(\cos\theta_p + \frac{\sin\theta_p}{\sin\theta_n} \cos\theta_\eta) - T_p)^2 - (p_p \frac{\sin\theta_p}{\sin\theta_\eta})^2\right]^{\frac{1}{2}}$$

The second expression for the mass used only the angles measured in the experiment:

$$XMN2 = \frac{2(f - \gamma_\eta)}{e^2 - (f - \gamma_\eta)^2} M_p$$

where

$$f = (\frac{\sin\theta_\eta}{\sin\theta_p} \cos\theta_p + \cos\theta_\eta) \beta_\eta \gamma_\eta,$$

$$e = \frac{\sin\theta_\eta}{\sin\theta_p} \beta_\eta \gamma_\eta,$$

and γ_η is calculated from the expression for β_η above.

The energy of the eta was then calculated in two independent ways: the first used the expression $E_\eta = M_\eta \gamma_\eta$ where γ_η was calculated as described above from the reaction plane information from the proton side together with the hodoscope information on the two decay γ-rays. The other method assumes an elastic p-C vertex: then from conservation of energy, we see that the energy of the η is just the photon energy minus the proton kinetic energy:

$$E_\eta = k_1 - T_p$$

where the calculations of k_1 and T_p are described above.

In practice, in the kinematical region in which we were working, this latter determination of the energy of the eta was very insensitive to the accuracy of the measurement of T_p, or to any inelasticities, up to about 30 MeV in the p-C vertex. Of course, the first mentioned determination of E_η is completely independent of the proton energy. The difference of these two quantities, called DELE, then ought to be near zero for true events, and relatively independent of p-C inelasticities.

In practice, for any particular setting, each event was plotted as in figure 3.1: the vertical axis of this dot plot is DELE, and the horizontal axis, XMN1, the mass of the meson. The true η events cluster in the center where expected; in addition, we see a rather broad background which is due primarily to $2\pi^o$ production and to the $3\pi^o$ decay of the η itself.

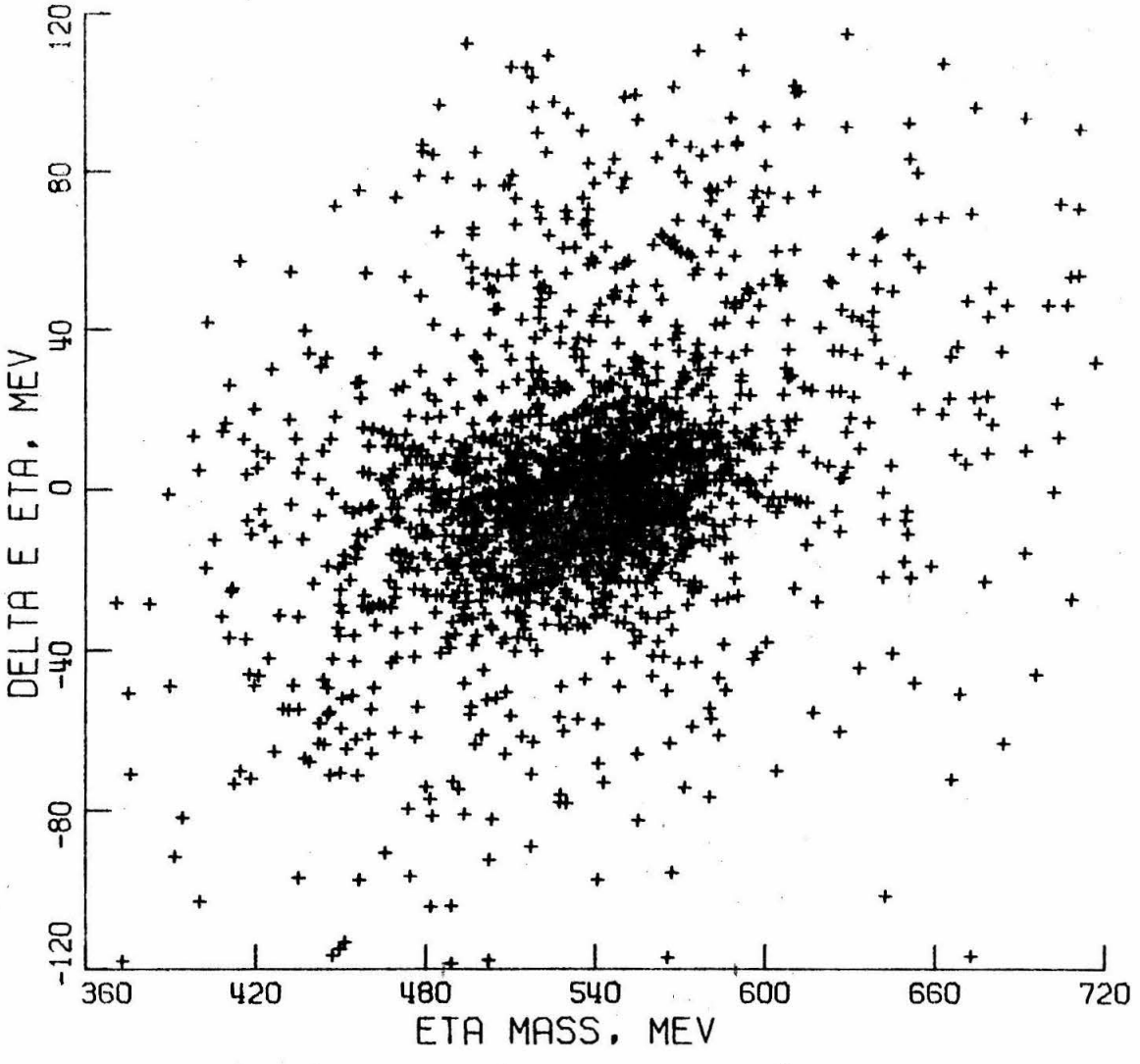

Figure 3.1 Mass vs. ΔE_η for events in Set I.

This method of exhibiting our events and then choosing η events to be those within the central cluster was the one which enabled us to use our overdetermination in the best way. If our reaction kinematics were exactly determined, then we could calculate the mass of the η (XMN1) and make a cut upon that variable; since in fact, disregarding any p-C inelasticities, we are one parameter overdetermined, we can apply just one more cut. Without assuming the mass of the eta, this cut would be on the variable XMN2, the other expression for the eta mass. The events were displayed on a dot plot with the axes being the two ways of calculating the eta mass, as we see in figure 3.2. We see from the figure an eta peak broader than that in figure 3.1 and with more background.

Other methods of separating foreground from background were tried: all were inferior to the method described of plotting the difference in two determinations of the eta energy against the eta mass. The reason for this is that the variable θ_η, the lab eta angle, appears only in the expression for XMN1 and not in that for DELE. For amusement, we show in figure 3.3 the results of an attempt to select foreground events without the use of the measured proton energy and thus to avoid the question of p-C inelasticities we plot k_2-k_3 against XMN2, all of which are independent of T_p, the proton kinetic energy.

To exhibit the size of our background more clearly, we show in figure 3.4 the projections of the indicated bands of events from the dot plot onto the mass and DELE axes. We again see peaks in both distributions where expected, with a broad background underneath. Choosing

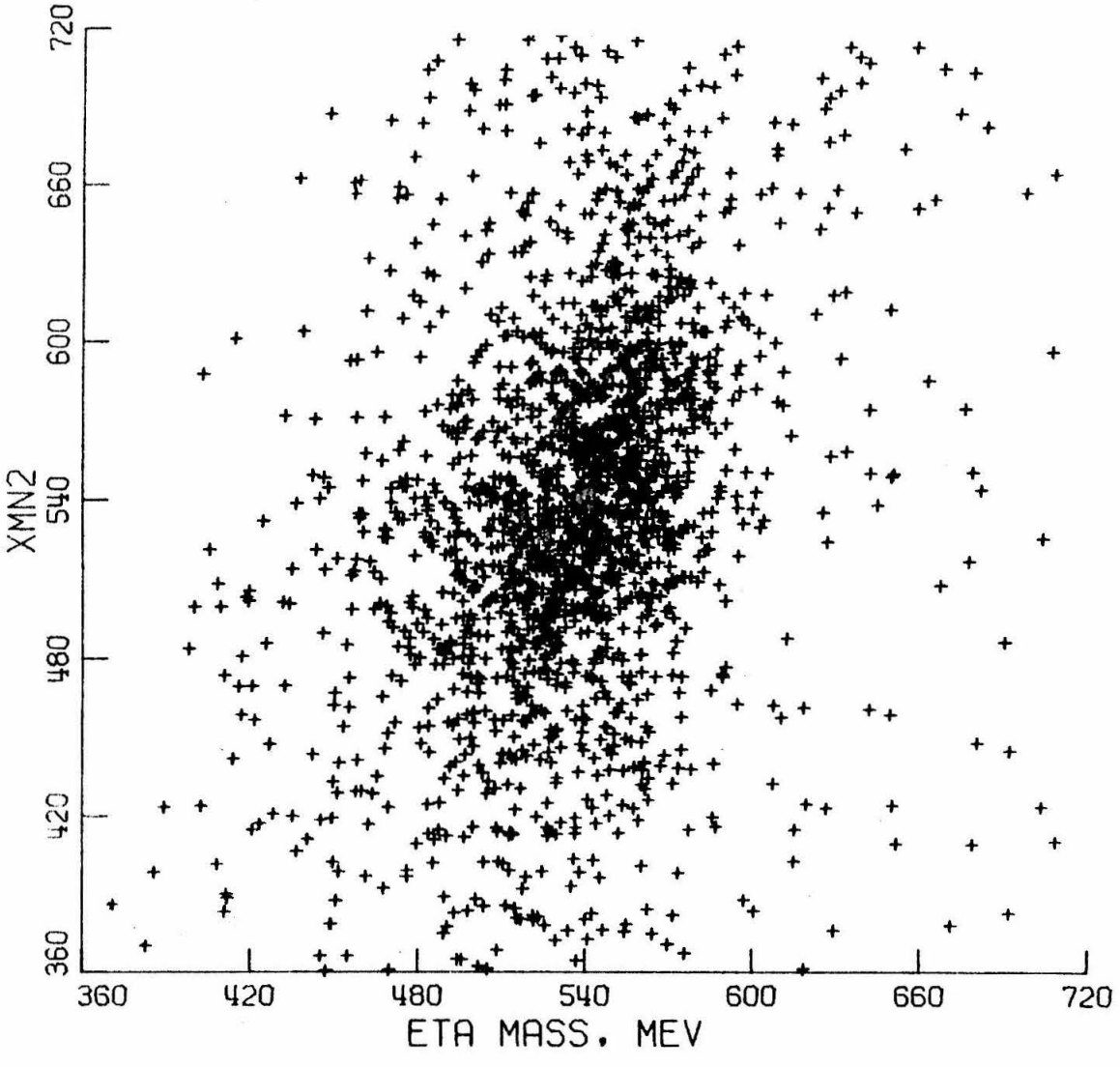

Figure 3.2 XMN1 vs. XMN2 for events in Set I.

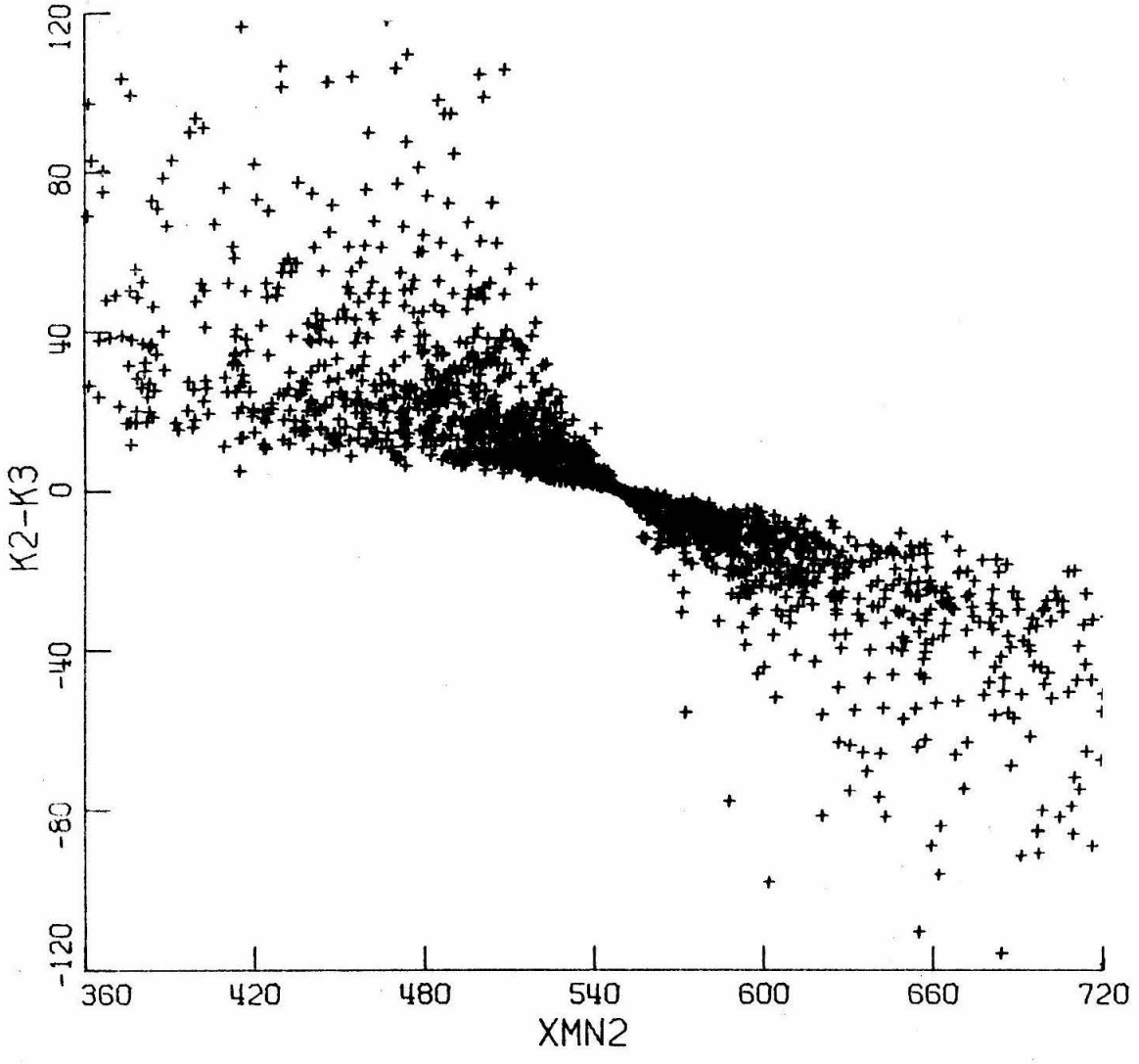

Figure 3.3 K2-K3 vs. XMN2 for events in Set 1.

events from the central cluster for analysis resulted, as we can see from Table 3.1 for this setting, in a cut of some 57 hundred events. Even so, roughly 15% of the events remaining were part of the background; at the end of this section, we will describe how the remainder of the events in the dot plot were used to make a correction for this contamination under the central cluster.

By using the information obtained from the two pulse-heights in the shower counters, we were able to exclude some 500 more background events from under the η peak for the setting in question. In figure 3.5 we see a pulse height spectrum from one shower counter for events under the central cluster as well as for events away from the cluster (background events). We see that the pulse heights for events associated with η production are generally much higher than those associated with background processes, indicating that the photons associated with the background are generally of lower energy. The calibrations of our shower counters will be described in Appendix VI-3; the cuts were made to maximize background discrimination without a significant loss of eta events.

We show in figure 3.6 a dot plot analagous to that shown in figure 3.1 where the present plot contains only events whose p-C scattering angle was less than 4°. This sample of events is one in which an overwhelming number of protons scatter purely elastically; because of the similarity of the two plots, we see that our selection procedure for η's is not visibly affected by p-C inelasticities.

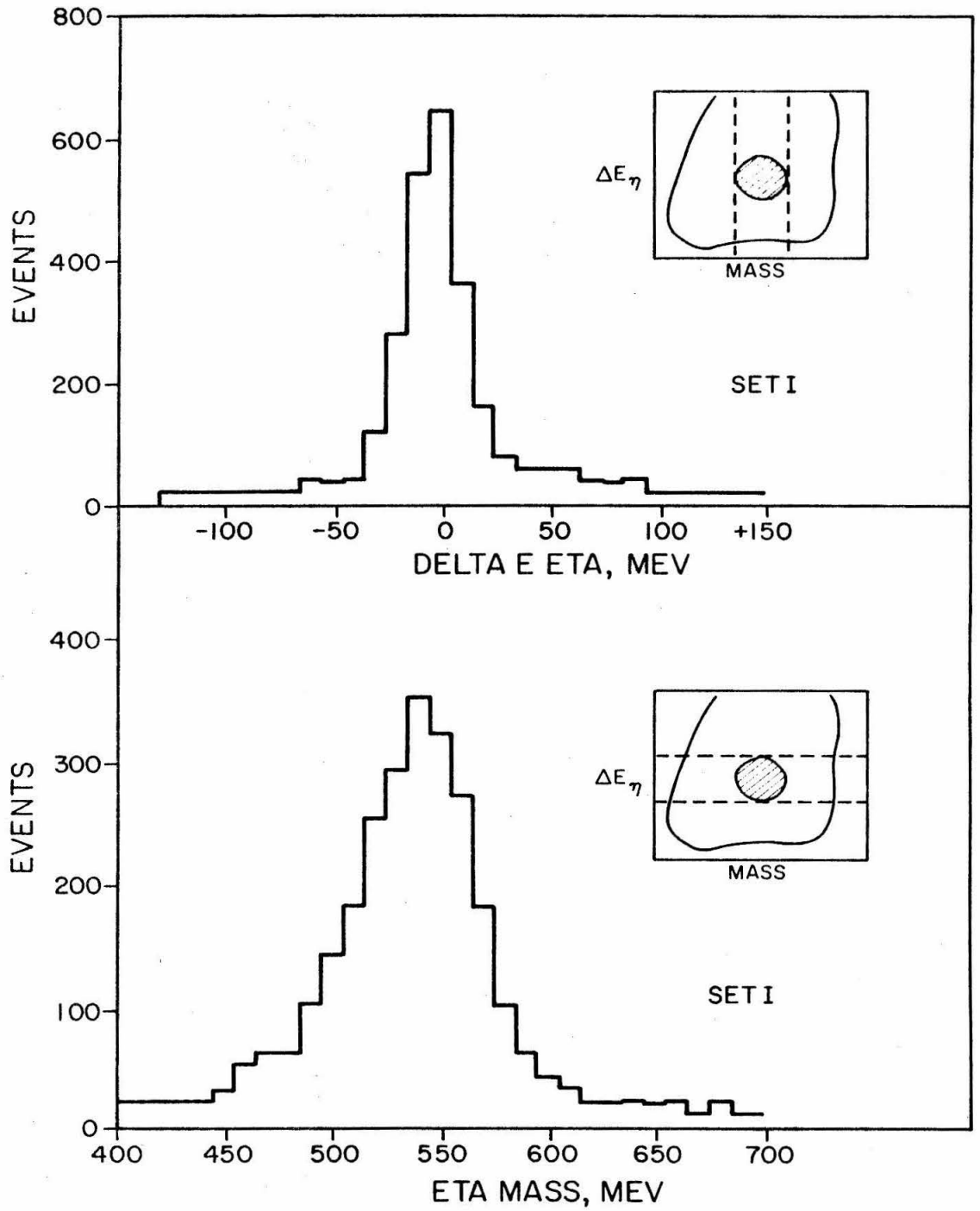

Figure 3.4 Mass and ΔE_η projections for events in Set I.

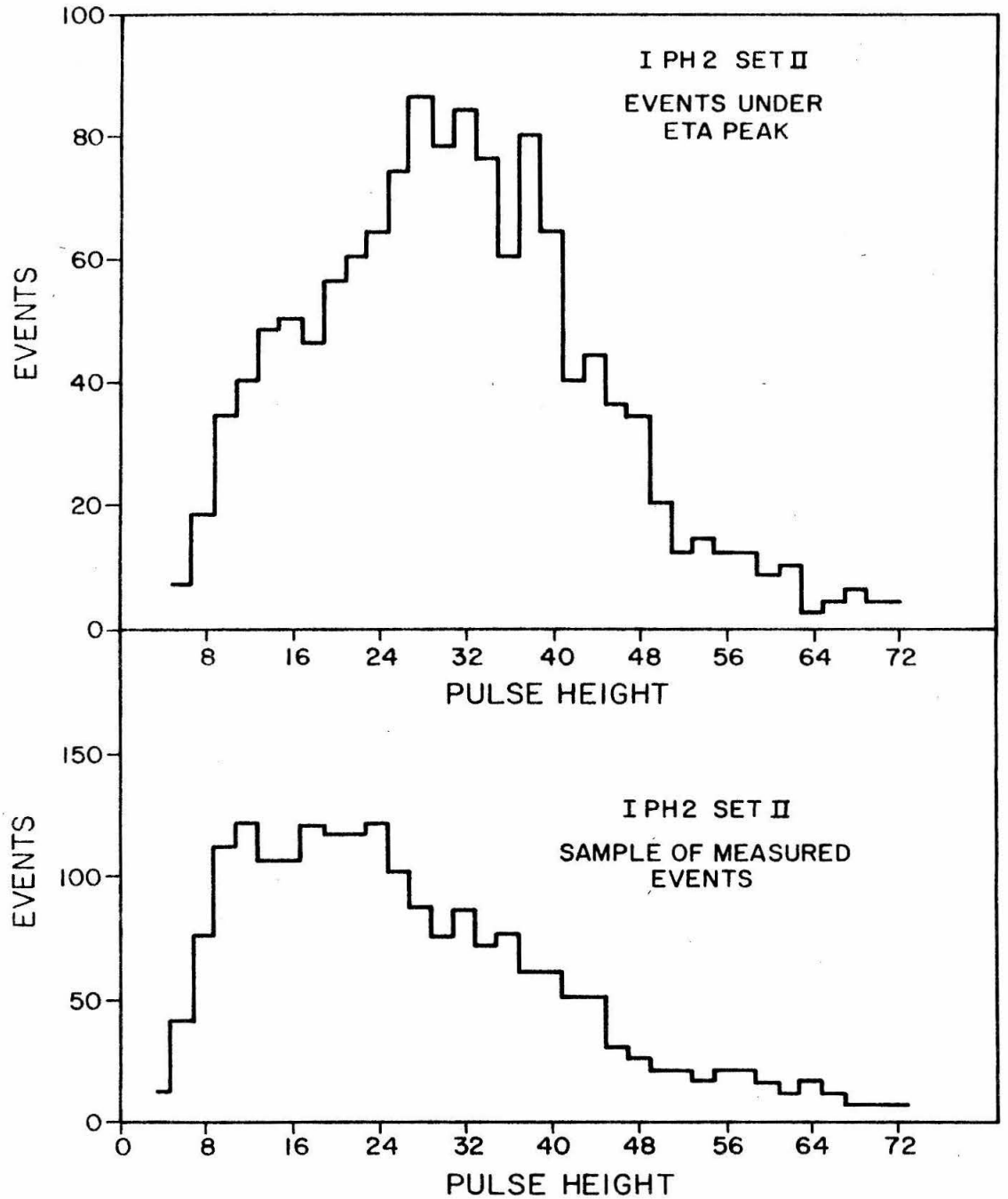

Figure 3.5 Pulse height distributions for events under η peak and for an uncut sample of events, Set II.

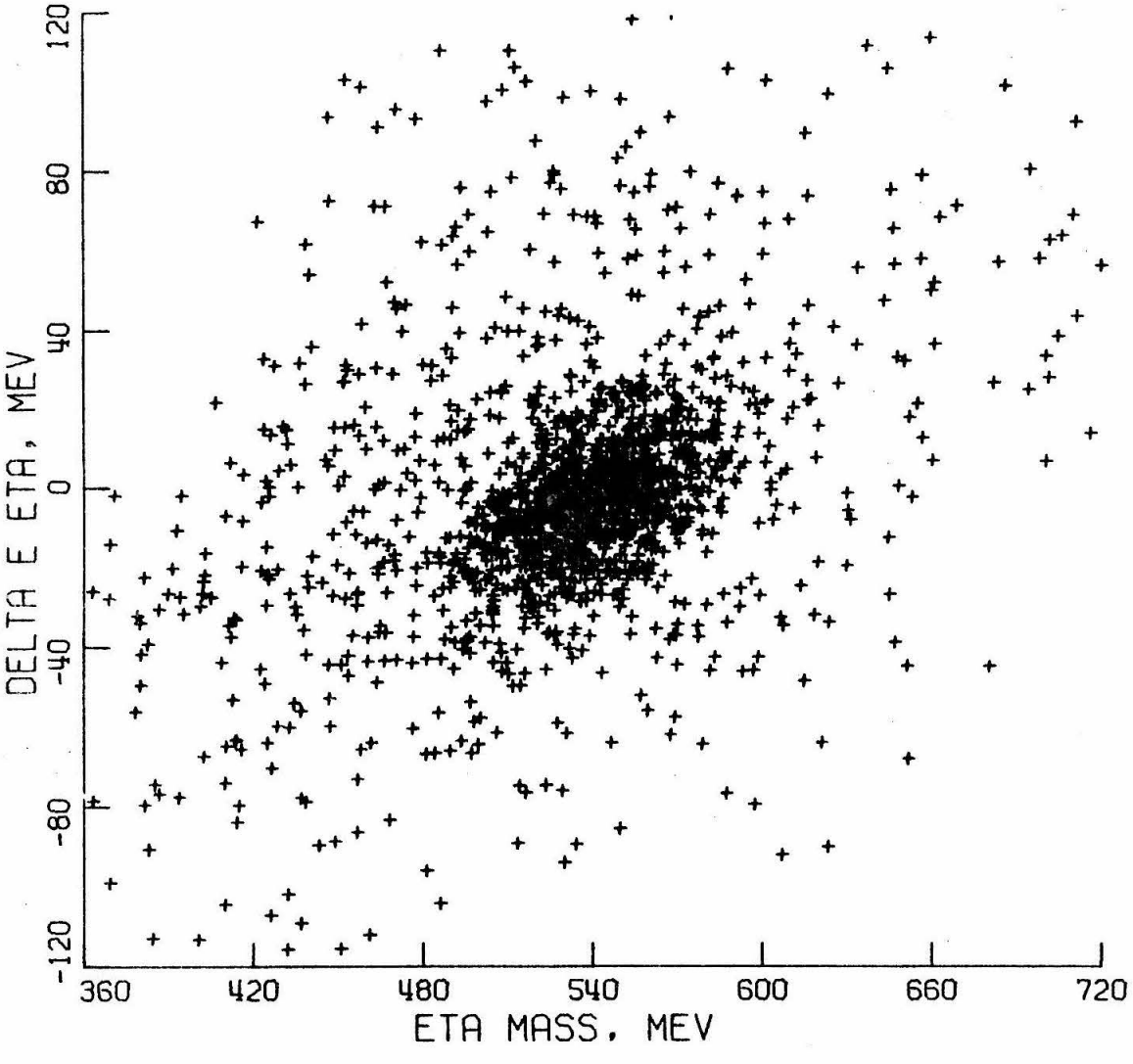

Figure 3.6 Mass vs. ΔE_η for p-C scatters $<4^\circ$ (highly elastic events).

4. Selection of "Useful" Scatters; Polarization Determination

The last five cuts in Table 3.1, responsible for eliminating some 2000 events, and leaving 1800 for analysis for this setting, all are concerned with the parameters characterizing the p-C scatter. These are the angle of the scatter and the energy after the scatter, determined by converting the proton range after the scatter to an energy.

The analyzing power of a p-C scatter is defined to be the fraction of 100% polarized protons scattering to the left in a left-right asymmetry determination. This number is of course a function of scattering angle, energy at the scatter, and the inelasticity of the scatter itself. A somewhat modified version of W. A. McNeely's[14] fit to the world's p-C asymmetry data was used in the present experiment. The fitting program before modification would yield an "experimental average" asymmetry when furnished the energy and angle of the scatter, the inelasticity of the scatter and the experimental (Gaussian) uncertainty in the inelasticity for the particular event. In the present experiment, we knew only the scattering angle and energy after the scatter, our resolution being too poor to reconstruct accurately enough the energy at the scattering vertex. The program was modified to account for our flat resolution in inelasticity (we knew only an upper limit on the inelasticity of a particular event beyond which its reconstructed mass would be too small to be considered as a good event), and our lack of knowledge of the energy at the vertex. The modified program was compared with the original program on a set of data from another experiment[15] where the inelasticities were well known and the results were found to be consistent.

These last five cuts on the data, then, are due simply to our lack of knowledge of the p-C analyzing power in certain regions: 208 events were discarded because their scattering angle exceeded 30° (lab)--a region where, for most energies, the analyzing power is either very small or changing very rapidly with angle, or not known well at all; 752 events were discarded because their projected scattering angle on the scanning table was less than 4°--a region where the analyzing power is small, Coulomb scatters begin to compete with nuclear scatters, and where we could not be certain of a lack of left-right scanner bias in the selection of events; 1031 events were discarded because their energy after the scatter was less than 90 MeV, a region where, for elastic events, the analyzing power is small and not well known. Finally, 25 events were not used because the analyzing power for these events was less than 0.1--a number comparable with the experimental uncertainties in p-C analyzing powers.

We are now left with, for this setting, 1793 p-C scatters to analyze, about 80% of which are associated with the photoproduction of the η. The events were binned according to the energy of the incoming γ ray and the center-of-mass η production angle. The analyzing power of each event was calculated using the above-mentioned fitting program, and the results, along with the recontructed ϕ of the p-C scatter, (see figure 2.4), were used in a maximum likelihood determination of the polarization. The method is described in Appendix VI-10; for now let us say if we have a bin of N events, the i'th event having analyzing power A_i and scattering angle ϕ_i (ϕ being 0° for a "left" scatter, 90° for an "up"

scatter, 180° for a "right" scatter, etc.)), then the likelihood function for this bin of events is:

$$L(P) = \frac{1}{(2\pi)^N} \prod_{i=1}^{N} (1 + A_i \, P\cos\phi_i)$$

This form of the likelihood function assumes that the detection efficiency for a p-C scatter is independent of ϕ; when plotted as a function of P, the most likely value of the polarization is that P at which L(P) is maximum. In most cases (and all for the present experiment) L(P) is very nearly a Gaussian and the width of the Gaussian can then be interpreted as the experimental error in the determination of P. L(P) is normalized in the following sense:

$$\int_0^{2\pi} \cdots \int_0^{2\pi} \int_0^{2\pi} L(P) \, d\phi_1 \, d\phi_2 \cdots d\phi_n = 1.$$

Thus the height of the likelihood function can also be interpreted. (See Appendix VI-10E).

In figure 3.7 we see a plot of one of our likelihood functions, corresponding to events within the central cluster in the dot plot of figure 3.1, for a particular bin in photon energy.

5. Background Subtraction

In practice, a polarization analysis was made on the "background" events away from the central cluster to adequately correct for background contamination under the central cluster. After our finding that the background or "off-kinematics" polarization did not vary significantly (within statistics) from quadrant to quadrant of the dot plot, all of the background events were lumped together and the resulting

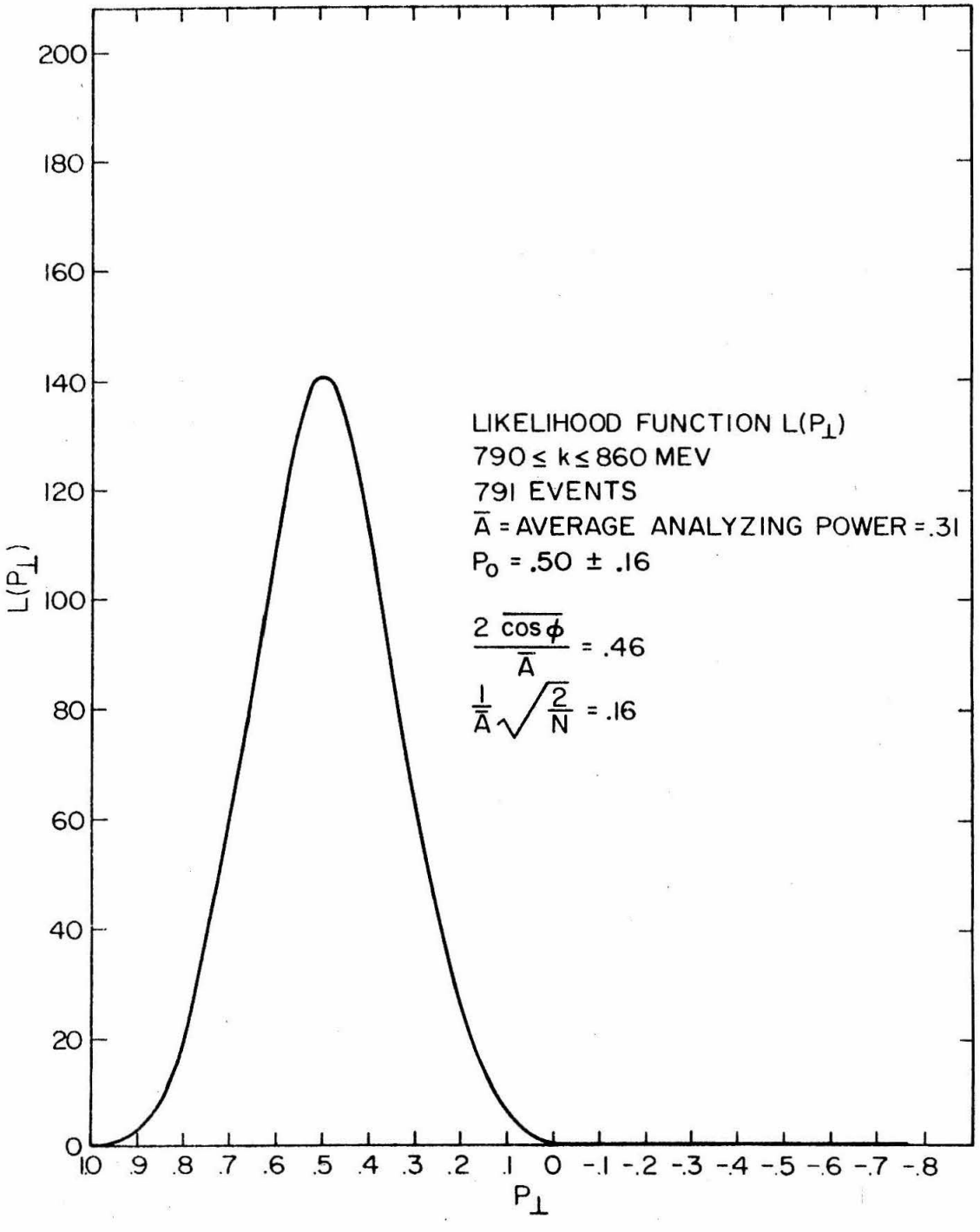

Figure 3.7 Typical likelihood function.

polarization was "subtracted", according to the fraction of background events in the central region.

The fraction of background events under the eta peak was determined by a method devised by L. S. Rochester[16] which will be described briefly here.

For events away from the central cluster, we made distributions of the following variables: the event origin, the proton range, the horizontal and vertical coordinates of the proton in the third counter in the proton telescope, and the horizontal and vertical coordinates of the photon in each photon detector. We assumed and found that these distributions (for the events away from the eta peak) were uncorrelated. Points were selected at random from these distributions and the "event" was run through our analysis program, generating a simulated background event. The process was repeated for sufficient statistics. Figure 3.8 shows a dot plot of these generated events, analagous to figure 3.1. In figure 3.9 we see distributions of these generated background events in the variables XMN1 and DELE with cuts made so that this figure is exactly analagous to figure 3.4. We normalized these distributions by requiring that, away from the region of the η, the distributions of real events and of generated events would contain the same number of events. Then we knew, in two independent and agreeing ways (using the distributions in DELE or in XMN1) how many background events were under the eta peak; and by comparing the distribution in photon energy for our generated background events with that of our real events, we knew our background contamination for any desired bin in photon energy.

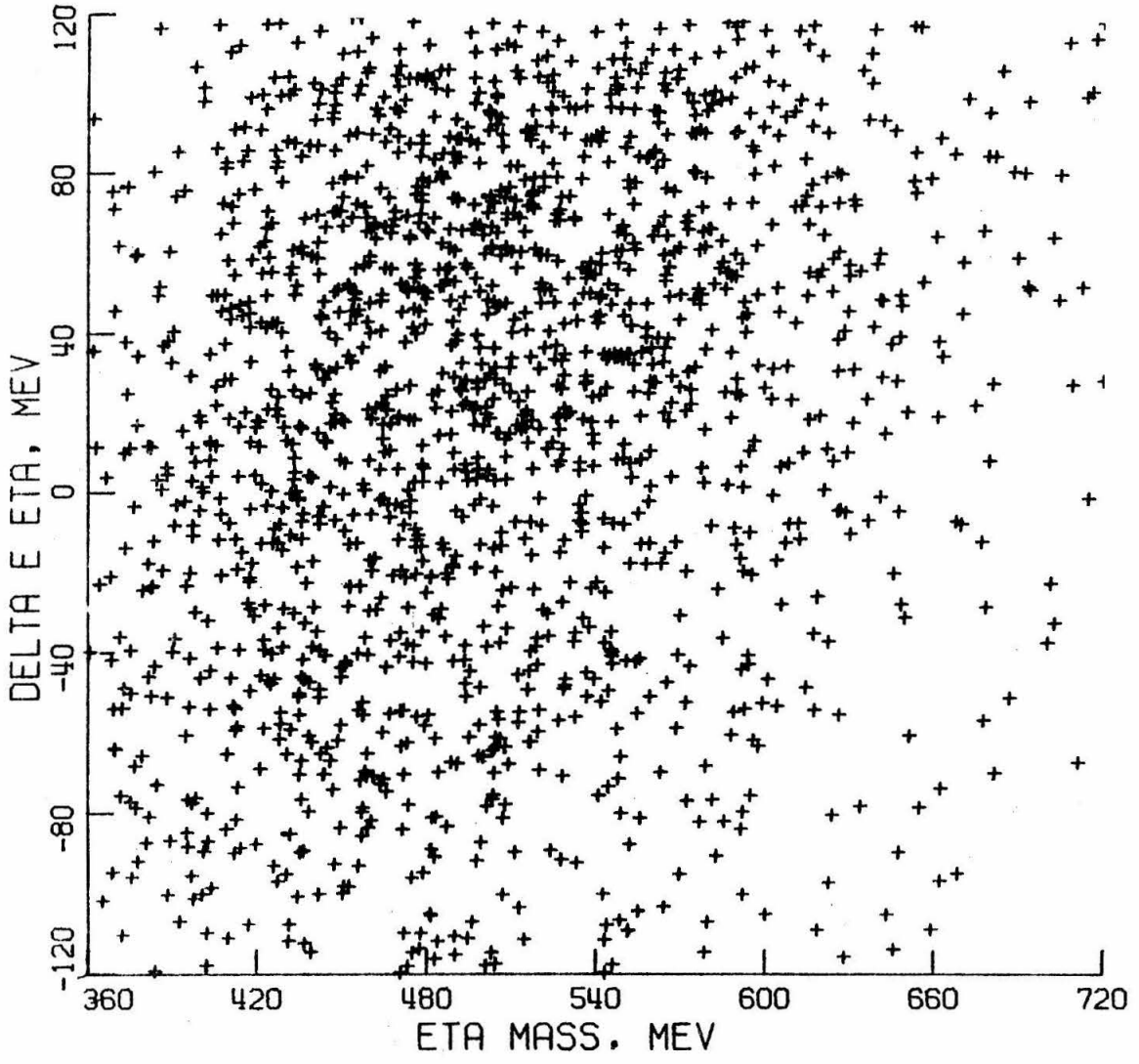

Figure 3.8 Mass vs. ΔE_η for generated background events, Set I.

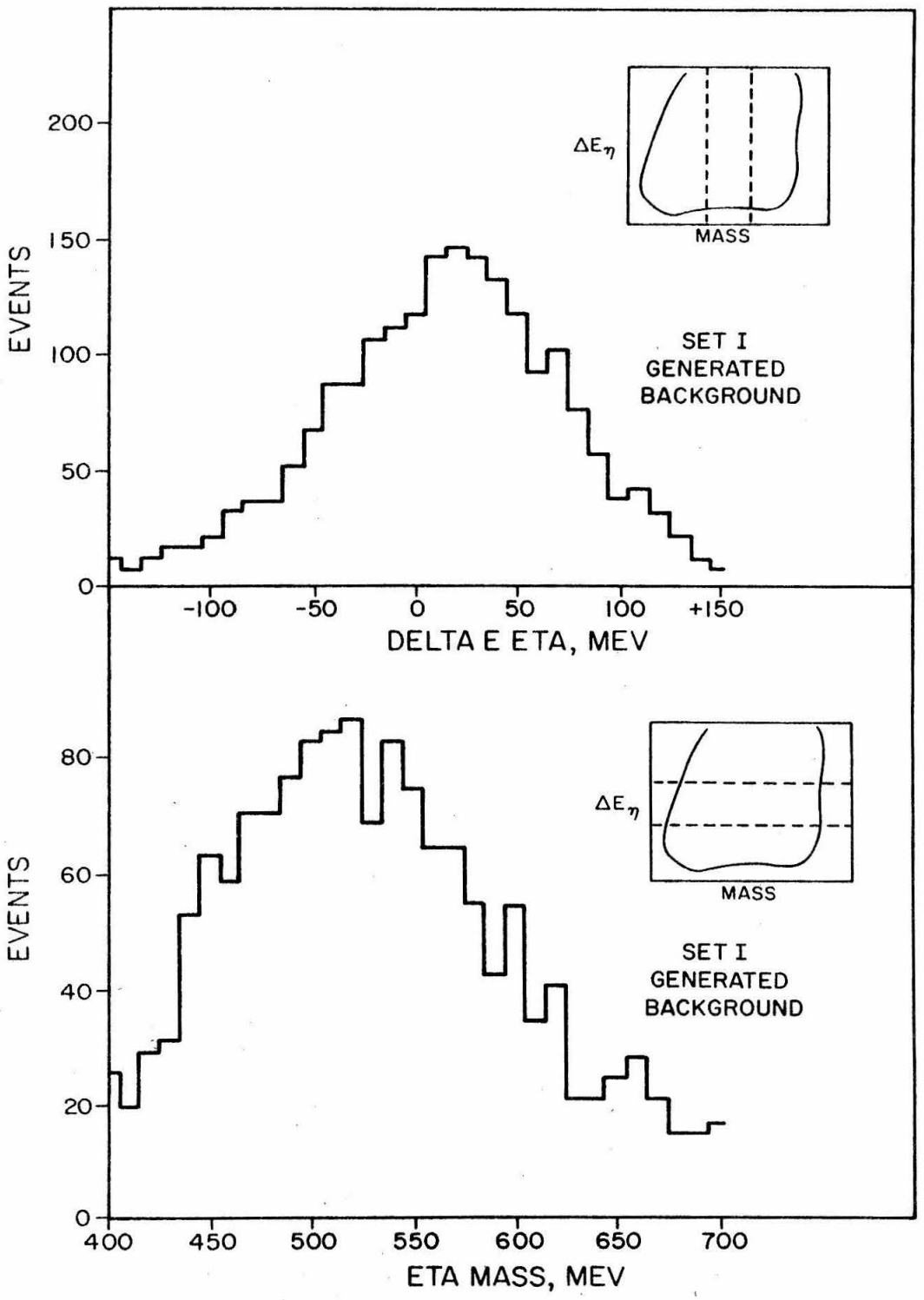

Figure 3.9 Mass and ΔE_η projections for generated background events, Set I.

We then performed the required subtractions in the polarization values; to repeat, our only assumptions being that the energies and angles of the proton and photons of the real background events are uncorrelated, and that the polarization of background events under the eta peak is the same as its average value around the eta peak.

6. Determination of Polarization in the Reaction Plane

By exactly the same methods, the polarization in the plane of the reaction was determined. This time, the likelihood function is:

$$L(P_\perp, P_\parallel) = \frac{1}{(2\pi)^N} \prod_{i=1}^{N} (1 + A_i (P_\perp \cos\phi_i + P_\parallel \sin\phi_i))$$

where $P_\parallel$ is the polarization in the reaction plane, and $P_\perp$ the polarization perpendicular to the reaction plane. $P_\parallel$ ought to be zero by parity conservation, (see Appendix VI-9). A non zero $P_\parallel$ would indicate perhaps a scanning bias or other error in our methods. $P_\parallel$ was found to be consistent with zero where required, as the next section indicates.

IV. RESULTS

By the methods described in the previous section, polarization values perpendicular to as well as in the reaction plane were calculated for five bins in photon energy.

Figure 4.1 shows the spectrum of photon energies for events within the central clusters for both Set I and Set II. In figure 4.2, we see our distributions in center-of-mass production angle, calculated from the proton energy and angle, for the same sets of events. Both the distribution in photon energy and in center-of-mass production angle contain some background events, 30% for Set I and 27% for Set II.

In tables 4.1 - 4.4, we have tabulated our results; we have explicitly shown the size of the background correction for each bin in photon energy. No cut was made in center-of-mass production angle, figure 4.2. The values at the far right of these tables, then, are the polarization values and errors, corrected for background by the method described in Section III.

We note the agreement in the value of $P_\perp$ for the bin which the two settings have in common, $930 < k < 1000$ MeV. In figure 4.3, we have plotted our results for $P_\perp$ for the whole experiment, where we have lumped the events in the overlapping bin together. In doing this, we remember that the average center-of-mass production angles for Set I and Set II are 95° and 80°, respectively, figure 4.2.

We have similarly plotted our final results for $P_\parallel$ foreground events, $P_\perp$ background events and $P_\parallel$ background events in figures 4.4, 4.5 and

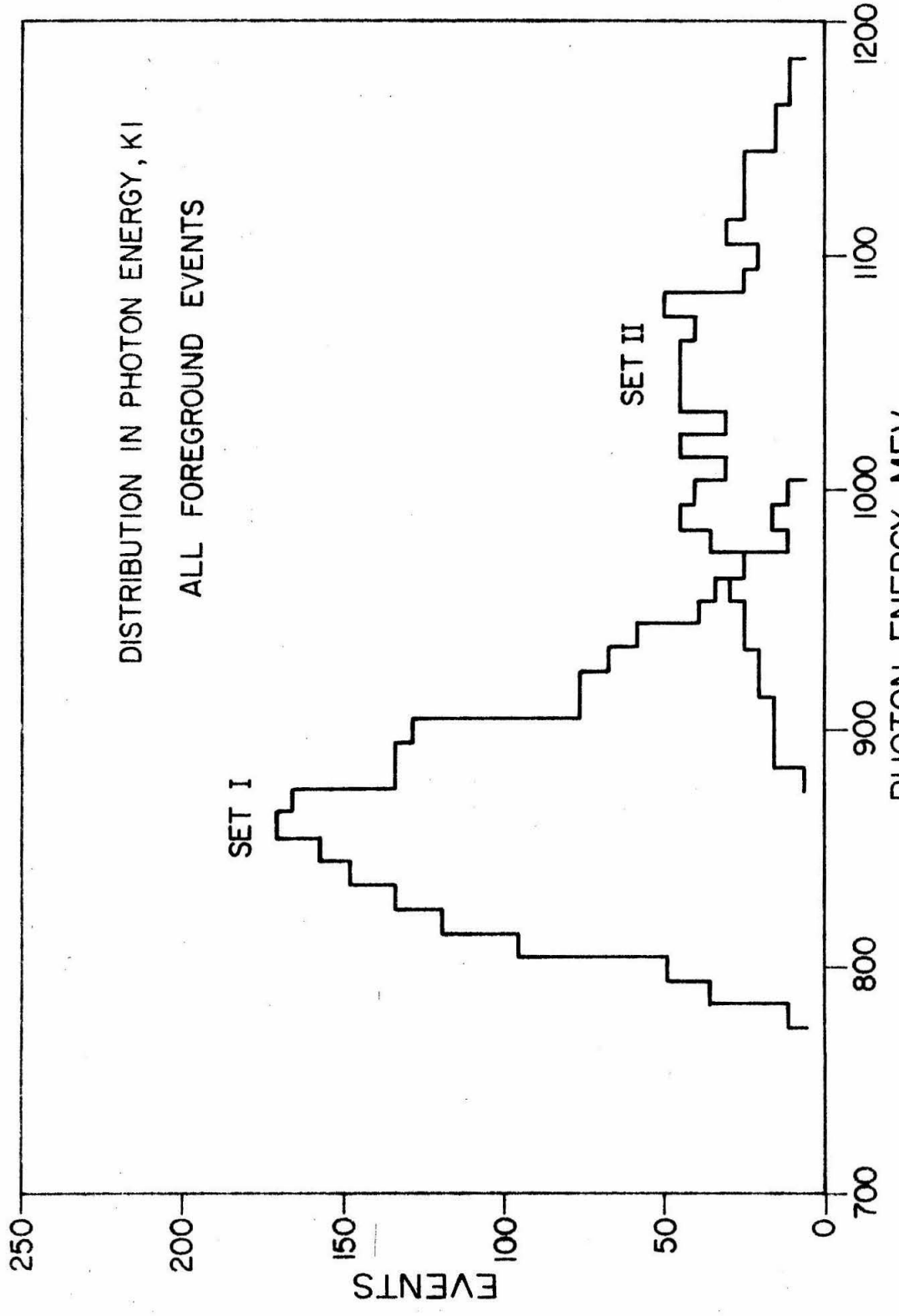

Figure 4.1 Distributions in photon energy for central cluster events (includes 30% background events).

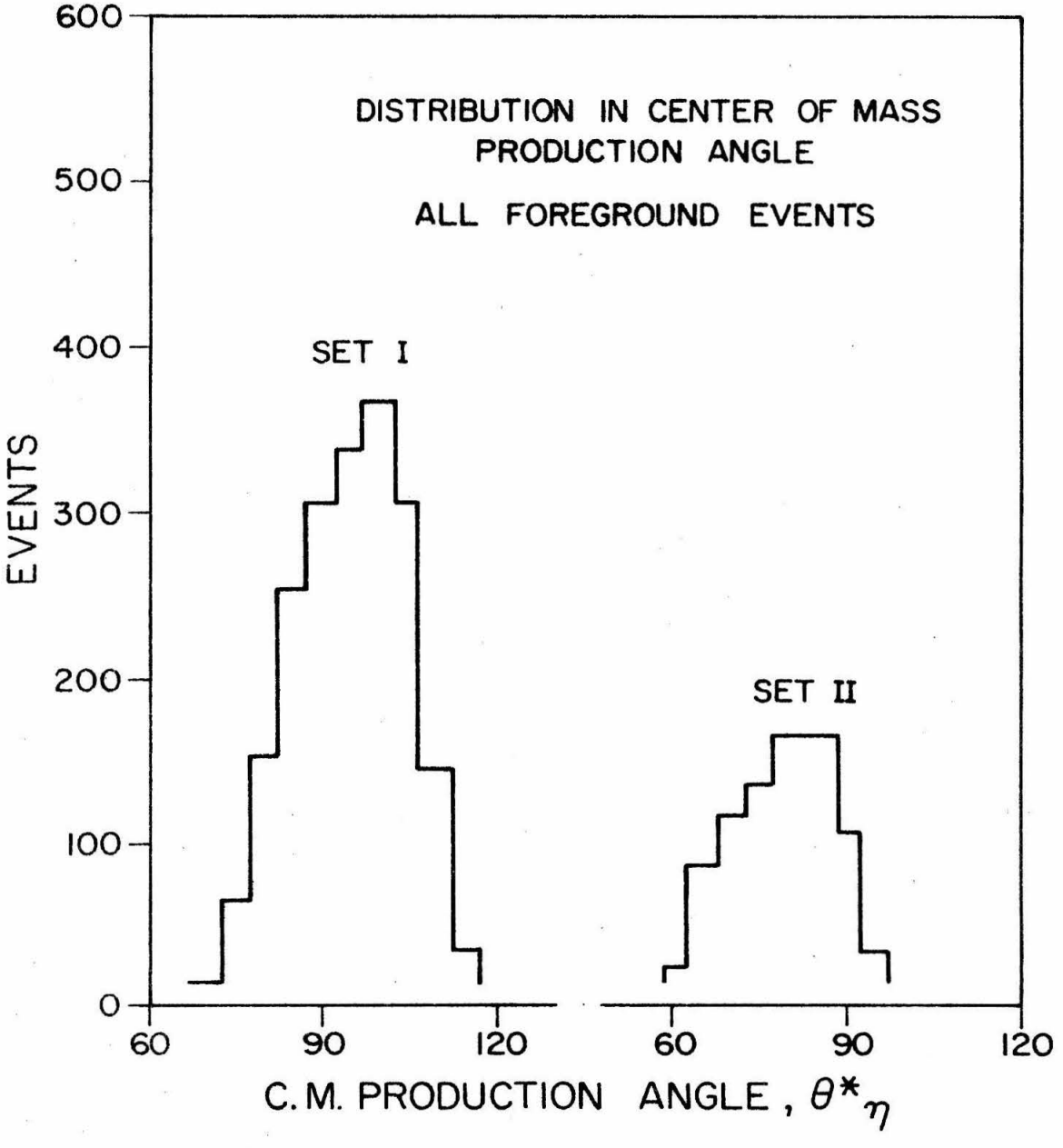

Figure 4.2 Distributions in center-of-mass production angle for central cluster events (includes 30% background events).

Table 4.1

POLARIZATION RESULTS FOR SET I, $P_\perp$

$\langle k \rangle$ = 850 MeV $\quad \langle \theta_\eta^* \rangle = 90^\circ$

K MeV	P_{cc}	ΔP_{cc}	Events	$\bar{A}$	P_b	ΔP_b	Subtracted Events	$P_\perp^\eta$	$\Delta P_\perp^\eta$
790- 860	.50	±.16	791	.31	.13	±.14	322	.64	±.22
860- 930	.15	±.14	811	.35	.22	±.14	176	.14	±.17
930-1000	.69	±.21	191	.43	.28	±.22	35	.75	±.24

In this table and the following ones P_{cc} and ΔP_{cc} are the values of the polarization and its error for the events within the central cluster of figure 3.1 . P_b and ΔP_b are the values of the polarization and its error for the background events away from the central cluster of figure 3.1. $\bar{A}$ is the average analyzing power for each bin of events. $P_\perp$ is in the direction of $\vec{k}x\vec{q}$ where $\vec{k}$ is the photon momentum and $\vec{q}$ is the meson momentum.

Table 4.2

POLARIZATION RESULTS FOR SET I, $P_{\parallel}$

$\langle k \rangle$ = 850 MeV $\quad \langle \theta_{\eta}^{*} \rangle = 90^{\circ}$

K MeV	P_{cc}	ΔP_{cc}	Events	$\bar{A}$	P_b	ΔP_b	Subtracted Events	$P_{\parallel}^{\eta}$	$\Delta P_{\parallel}^{\eta}$
790- 860	.03	±.15	791	.31	-.13	±.14	322	.09	±.22
860- 930	-.04	±.14	811	.35	.10	±.15	176	-.06	±.17
930-1000	.52	±.21	191	.43	-.14	±.20	35	.61	±.23

Table 4.3

POLARIZATION RESULTS FOR SET II, $P_\perp$

$\langle k \rangle$ = 1050 MeV $\quad \langle \theta_\eta^* \rangle = 80^\circ$

K MeV	P_{cc}	ΔP_{cc}	Events	$\bar{A}$	P_b	ΔP_b	Subtracted Events	$P_\perp^\eta$	$\Delta P_\perp^\eta$
930-1000	.63	±.34	188	.31	.44	±.17	61	.66	±.39
1000-1070	.24	±.25	245	.36	.15	±.18	64	.25	±.28
1070-1140	.59	±.23	165	.41	.05	±.24	36	.64	±.26

Table 4.4

POLARIZATION RESULTS FOR SET II, $P_{\parallel}$

$\langle k \rangle$ = 1050 MeV $\quad \langle \theta_{\eta}^{*} \rangle = 80^{\circ}$

K MeV	P_{cc}	ΔP_{cc}	Events	$\bar{A}$	P_b	ΔP_b	Subtracted Events	$P_{\parallel}^{\eta}$	$\Delta P_{\parallel}^{\eta}$
930-1000	.32	±.34	188	.31	.13	±.19	61	.34	±.39
1000-1070	.00	±.23	245	.36	-.10	±.18	64	.01	±.26
1070-1140	.15	±.27	165	.41	.09	±.21	36	.15	±.30

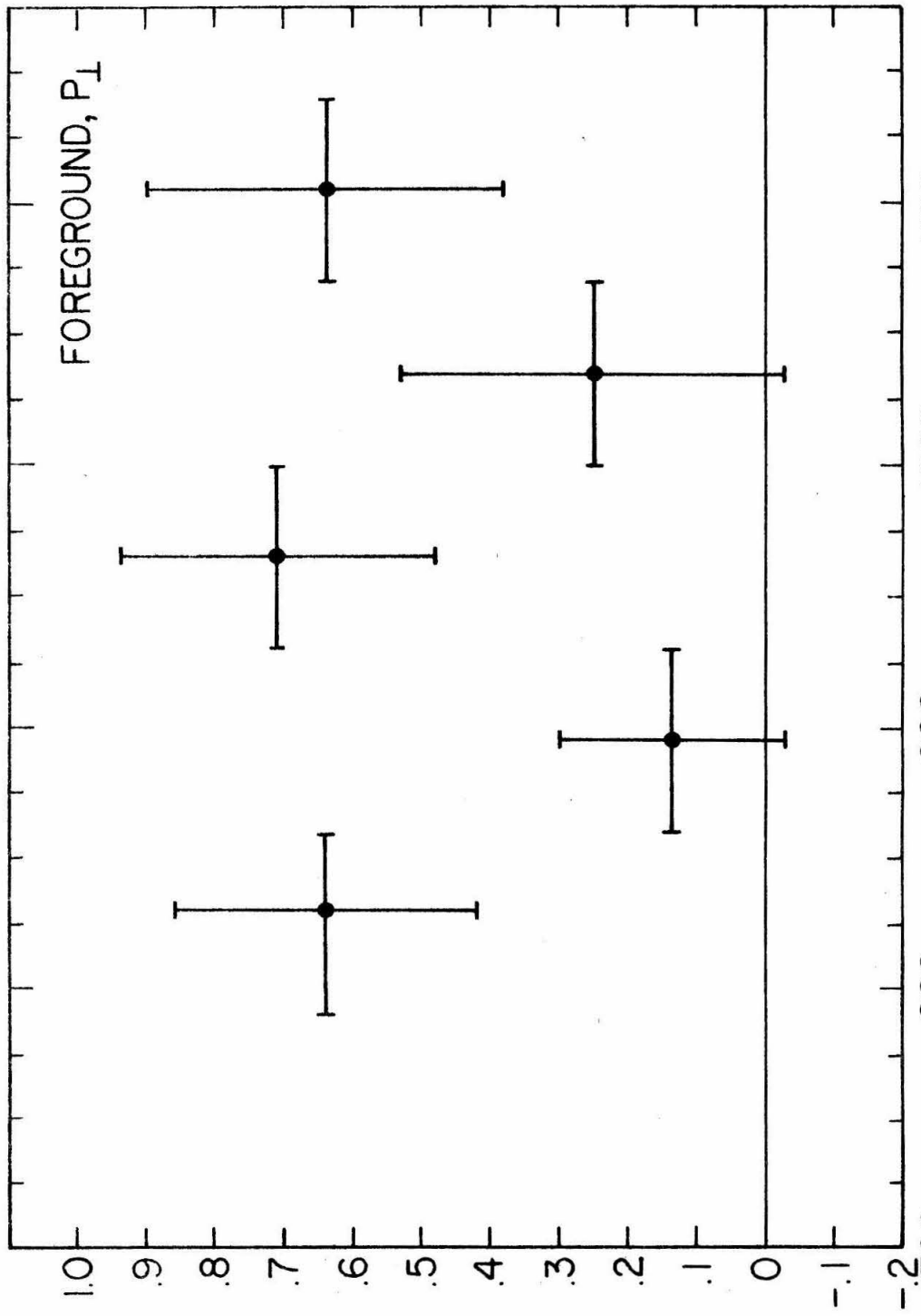

Figure 4.3 Recoil proton polarization perpendicular to the reaction plane in eta photoproduction.

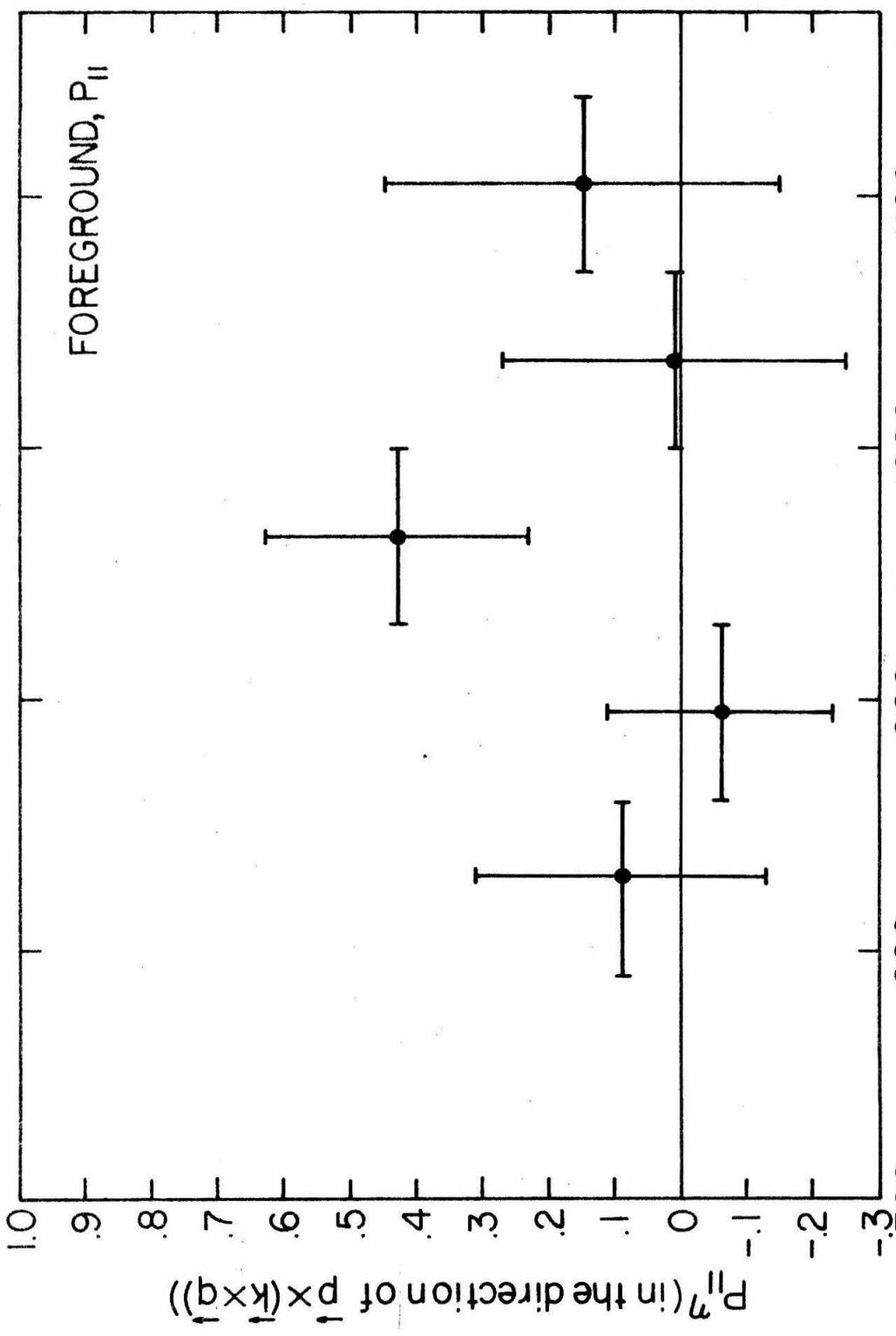

Figure 4.4 Recoil proton polarization within the reaction plane in eta photoproduction.

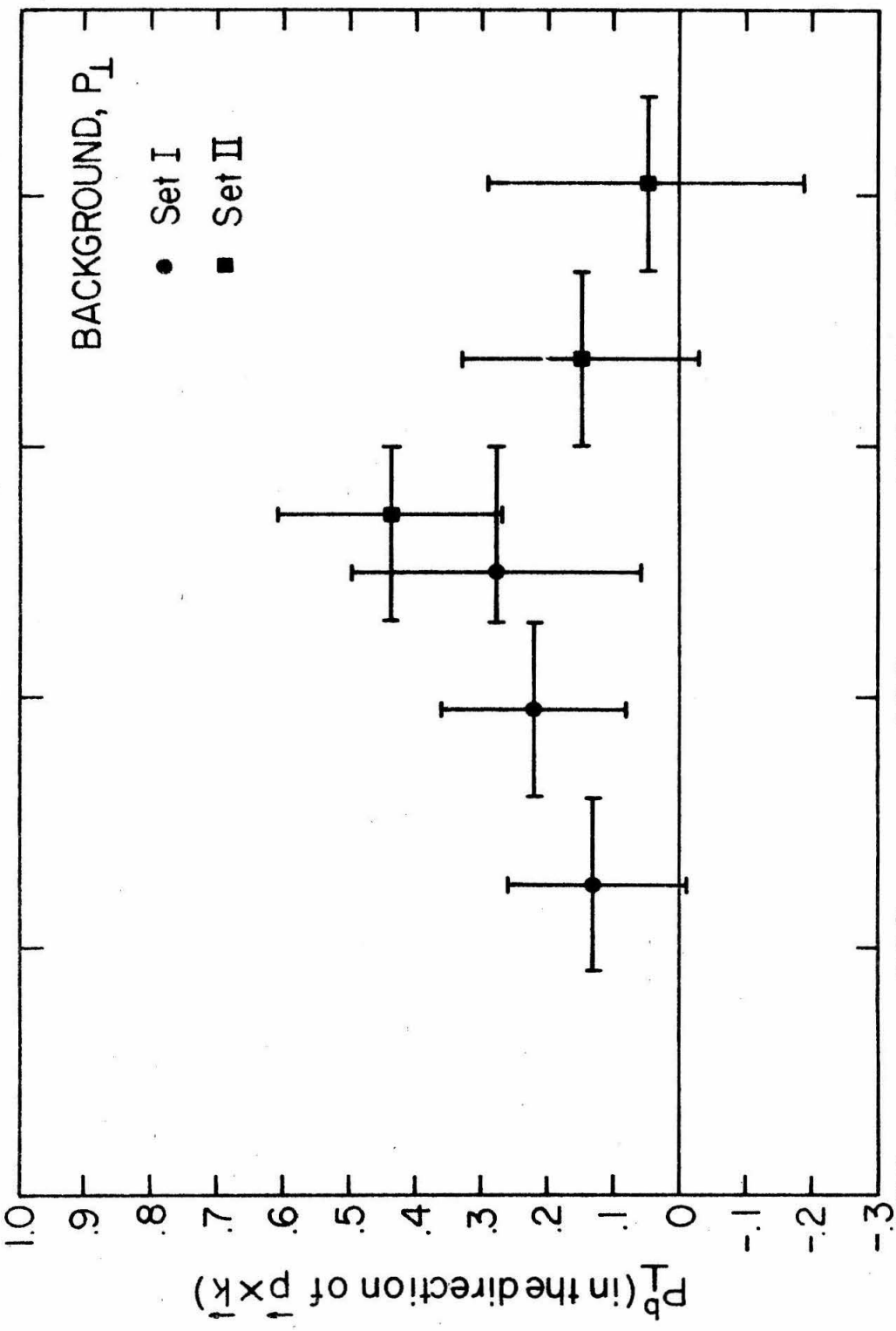

Figure 4.5 Background polarization, $P_\perp$.

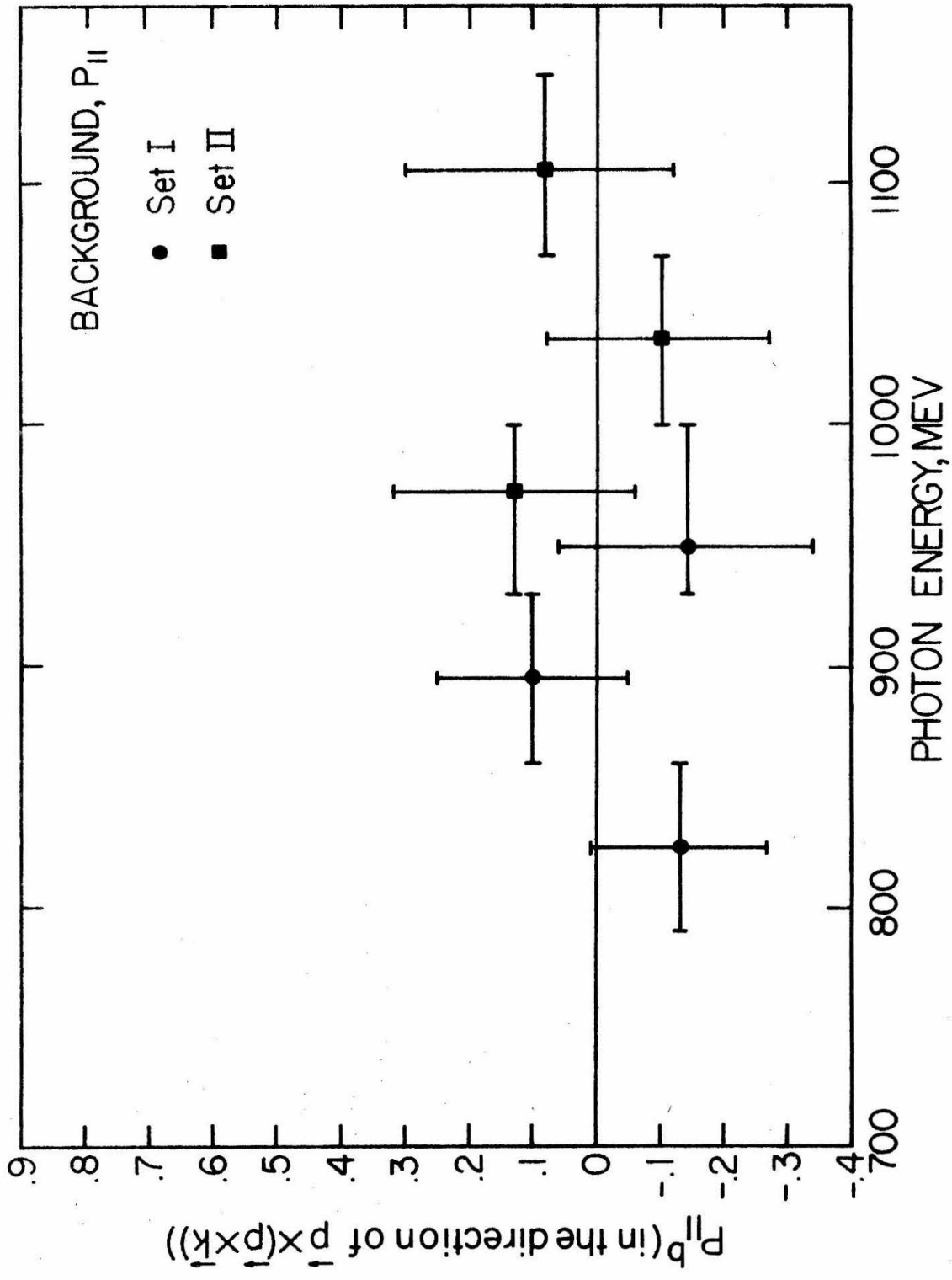

Figure 4.6 Background polarization, P_{II}

4.6, respectively. We note that there is no parity argument forbidding a background polarization "in the reaction plane" for a background process with more than two independent final state particles, Appendix VI-9. The reaction $\gamma p \rightarrow p\pi^o\pi^o$ is such a process, and we believe it to be the major source of our background.[17] The process

$$\gamma p \rightarrow p\eta$$
$$\qquad\quad \hookrightarrow 3\pi^o$$

also contributes to our background; of course for it we expect $P_{\parallel}$ to vanish.

The errors shown are statistical in nature. Possible sources of systematic errors such as analyzing power inaccuracies or shifts in measured quantities (range measurements, angles) have been investigated and it was found that the only major source of such errors was the reflection of our lack of knowledge of the inelasticities in the determination of the analyzing power for each p-C scatter. On the average, using the method devised of averaging the analyzing power over all possible inelasticities, our polarization values were changed by 20% over the results obtained by assuming each event to be purely elastic. (See Appendix VI-8.) By taking a careful look at the distribution of incoming proton energies for our experiment as well as the dependence of the p-C analyzing power and cross-section on inelasticity, we feel that the 20% number is reasonable and that our possible systematic uncertainty ought to be at the most 10% of the values obtained by assuming each event to be elastic. Thus we can say our systematic error

at each point is well within the statistical error bars themselves. We remark that for an experiment where incoming proton energies exceed those in our experiment significantly (an average of 165 MeV for Set I, 216 MeV for Set II), knowledge of the inelasticity becomes essential in doing an accurate polarization experiment.

A word should be said concerning the value of the polarization of the foreground parallel to the reaction plane for the bin k = 930 to 1000 MeV in Set I. This particular bin has a corrected (for background) number of events of only 156 whereas the other two bins at the same setting have a total of 1114 corrected events. Putting all of those events into one bin yields a polarization in the plane value for Set I of .09 ± .12. Similarly, for Set II the value of P in the plane is .15 ± .17. For the entire experiment, P in the plane for foreground events becomes .11 ± .10. This may be compared with the value of .46 ±.10, the polarization of foreground events out of the plane for the entire experiment.

V. DISCUSSION

Our results, as shown in figure 4.3, show a sizeable positive polarization both in the energy region dominated by the isobar $S_{11}(1550)$ and in that of the $P_{11}(1750)$ state. (See figure 1.1)

In this section, we would like to explore the following questions: (1) what would we expect the polarization to be in the simplified model where only the $S_{11}(1550)$ and $P_{11}(1750)$ resonances contribute; (2) from our data, what can be said about the P-wave amplitude under the $S_{11}(1550)$ and the S-wave amplitude in the region of the $P_{11}(1750)$; (3) were the $P_{11}(1460)$ photoexcited, how would the polarization and asymmetry behave; and (4), what conclusions about the isobars contributing to our reaction will we be able to reach when we have our data on the 0° - 180° asymmetry in eta photoproduction?

1. Polarization in the Model of the $S_{11}(1550)$ and $P_{11}(1750)$

If we consider only $j = \frac{1}{2}$ S and P wave meson-nucleon states, then from the conservation of parity, electric dipole absorption leads to the S_{11} intermediate state, and magnetic dipole absorption to the P_{11} intermediate state. We call the amplitudes for these absorptions E_d and M_d, respectively. Considering only these states, the expression for the differential cross-section for $\gamma p \rightarrow p\eta$ is

$$I(\theta) = |E_d|^2 + |M_d|^2 + 2\ \mathrm{Re}\ (E_d\ M_d^*)\ \cos\theta.$$

The recoil proton polarization, $P(\theta)$, for the above reaction, can be found from the following expression:

$$P(\theta)\, I(\theta) = -2\, I_m\, (E_d\, M_d^*)\, \sin\theta$$

where $\vec{P}(\theta)$ is in the direction of $\vec{k}\times\vec{q}$.

If we now define, (where R and I refer to real and imaginary parts)

$$A = \mathrm{Re}\, (E_d\, M_d^*) = E_R\, M_R + E_I\, M_I$$

$$\text{and} \quad P = -I_m\, (E_d\, M_d^*) = E_R\, M_I - E_I\, M_R, \qquad 5.1$$

then we see that the $0^\circ - 180^\circ$ asymmetry is given by

$$I(0^\circ) - I(180^\circ) = 4A,$$

and the polarization at 90° becomes

$$P(90^\circ) = \frac{2P}{|E_d|^2 + |M_d|^2}.$$

Now let us suppose that the S wave amplitude is resonant, corresponding to an intermediate state $S_{11}(1550)$. This assumption tells us something about the energy dependence of the E_d amplitude; at least near resonance, it should behave like

$$E_d \propto \frac{\Gamma/2}{E_r - E - i\,\Gamma/2} \qquad 5.2$$

where E_r is the energy of the resonance and Γ is its total width, about 120 MeV.

We see from the form for E_d that at the energy of the resonance,

$$\text{Re } E_d(1550) \approx 0. \qquad 5.$$

We also note that Im E_d takes on its maximum right at the energy of the resonance, which corresponds to $k = 830$ MeV.

If we similarly suppose the P wave amplitude to arise from the $P_{11}(1750)$ resonance alone, with a width of about 250 MeV, then we can make similar statements about its energy behavior.

We assume here that in the expression for the amplitude for $\gamma p \to p\eta$, the Breit-Wigner forms for the two resonances, $S_{11}(1550)$ and $P_{11}(1750)$, enter with undetermined relative sign only. This is a less stringent assumption than that used for the cross-section fits in reference 24. Then we see from our expressions for A and P that at 830 MeV, where $E_R \approx 0$, the asymmetry and the polarization should be opposite in sign.

2. S-P Interference in the Region of the $S_{11}(1550)$ and $P_{11}(1750)$.

Our polarization is positive at $k = 830$ MeV (the center of the $S_{11}(1550)$ resonance). Looking at expression 5.1 for the polarization, and remembering that E_R, the real part of the electric dipole amplitude, at this energy is zero, we can thus say that M_R, the real part of the magnetic dipole amplitude, is negative at $k = 830$ MeV. This magnetic dipole amplitude could result from the $P_{11}(1460)$.

Similarly our positive polarization at $k = 1100$ MeV implies either a positive real part to the electric dipole amplitude there, or a large

negative imaginary part to the electric dipole amplitude. We assume the P wave amplitude near 1100 MeV comes from the $P_{11}(1750)$: there are in principle the two choices for the E_d amplitude, since 1100 MeV is about 40 MeV less than the center of the $P_{11}(1750)$, so that M_R does not vanish there. If we assume this E_d amplitude at 1100 MeV to be resonant, then our second choice, large negative imaginary part to E_d, is compatible with the $S_{11}(1710)$.' We should point out that the central energies for the resonant states we are here describing, $S_{11}(1710)$ and $P_{11}(1750)$, are not well established.

3. Photoexcitation of the $P_{11}(1460)$

The threshold for eta photoproduction is 1487 MeV in the center-of mass. Thus if the $P_{11}(1460)$ contributes to this process, it does so through its long tail: its width is about 200 MeV.

We take the most simple minded approach to the problem of a resonance below threshold, namely that the M_d amplitude for the $P_{11}(1460)$ is still of the Breit-Wigner form of expression 5.2. Then, from our expressions for the asymmetry and polarization, we see that at 830 MeV, P and A both ought to be of the same sign. However, such an approach may be unreasonable. The problem of an S-wave resonance below threshold has been investigated.[18] The treatment explicitly applies for potential scattering in an S state alone. The result is that for a bound state of energy $-\varepsilon$ (where $\varepsilon > 0$ and small), the scattering phase shift

is given by

$$\tan\delta_o = -\sqrt{\frac{E}{\varepsilon}}$$

where E is the energy of the scattered particle. We note that the above phase shift varies rapidly from π at threshold to $\pi/2$ for $E >> \varepsilon$. The important point is that a below threshold resonance may be felt in a way totally different from the usual phase shift behavior, which is from 0 to π.

This treatment will not apply to the Roper resonance below eta threshold because of its large width. We note, however, that this abnormal clockwise behavior of the phase shift has been seen in partial wave fits to K^-p scattering, there arising from the $\Lambda(1405)$, 30 MeV below threshold.[1]

4. Information from Other Experiments

From our polarization data, we have established a P wave amplitude in the region of the $S_{11}(1550)$ and an S wave amplitude in the region of the $P_{11}(1750)$. We have not been able to say whether or not these amplitudes are resonant.

From expression 5.1, we see that for our positive polarization to be a result of interference between the $S_{11}(1550)$ and $P_{11}(1750)$, these two resonances must contribute with opposite sign. This makes definite

---

[1] Ferro-Luzzi, private communication.

predictions concerning the energy dependence of the $0^\circ - 180^\circ$ asymmetry in eta photoproduction; data on this asymmetry which were taken by our group are presently being analyzed and should shed more light on the two regions of interest. Even so, it will probably be necessary to do the polarized target and polarized photon experiments mentioned in the introduction to completely settle the question of the SU(3) assignment of the $P_{11}(1460)$ and to establish whether there is $S_{11}(1550) - S_{11}(1710)$ mixing.

VI. APPENDIX

1. Synchrotron, beam, monitoring.

Figure 2.1 shows the main features concerning the photon beam before interacting in the hydrogen target. Electrons in the main ring, after being accelerated in a circle to endpoint energy, strike a thin tantalum target. The resulting photon beam was collimated and scraped at several points with the use of lead apertures. Before reaching the final scraper, the photon beam was allowed to pass through a permanent 3 kilogauss magnet (shown in the figure) to further reduce any charged particles in the beam. At the target, the beam cross-section was circular with a radius of 1.2 cm and its angular divergence was 4 milli-radians.

No absolute measurement of beam intensity was needed in the analysis of our experiment. However, during the actual running of the experiment, the beam intensity was monitored by use of a Wilson quantameter. This provided a means of checking the rates of all counters and important coincidence circuits in the experiment.

2. Hydrogen Target

The liquid hydrogen target used in this experiment is shown in figure 6.1 and has been described previously.[19] In the present experiment, the cylindrical mylar cup which contained the hydrogen was 20.0 cm in length and 3.8 cm in diameter and was oriented so that the beam passed along the cylinder axis. In the way of the beam was .012"

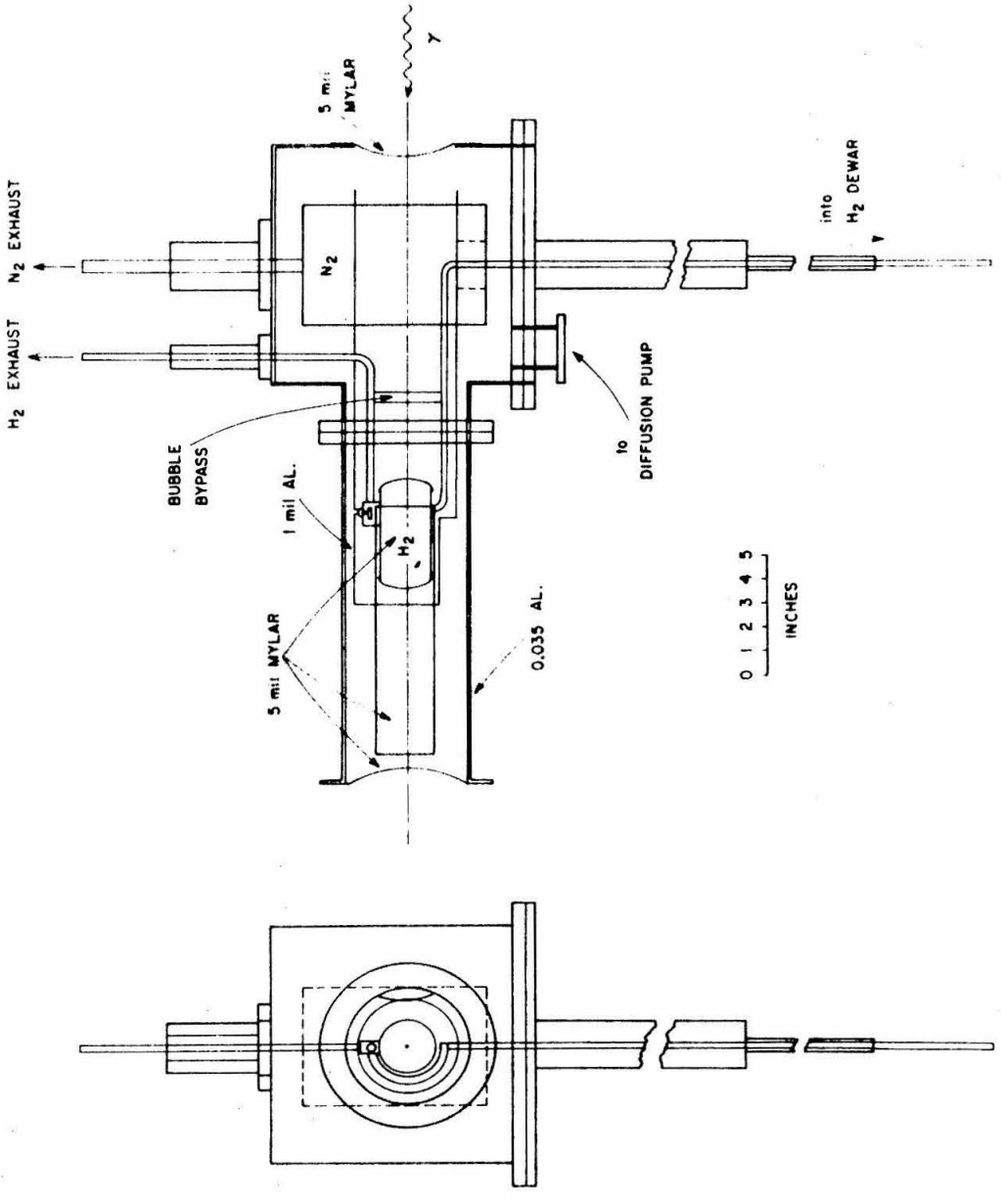

Figure 6.1 The hydrogen target.

of mylar (as well as the hydrogen--.0708 g/cm^3 at 20.3° K) and the reaction products went through (normally) .005" of mylar and .035" of aluminum after leaving the hydrogen.

3. Photon Detection

The apparatus used for photon detection in this experiment was similar to that used in previous experiments in our group.[20] Figure 6.2 shows two views of our detection system. Each detection system consisted of a veto scintillation counter to reject charged particles, two radiation lengths of lead in front of a 7 x 9 hodoscope grid of overlapping scintillation counters, and a lead-lucite Cerenkov shower counter. The total aperture of each system was 6" x 10" and for both kinematical settings, each was at a distance from the hydrogen target of about 22". The hodoscope grid consisted of five overlapping vertical counters yielding nine bins, and four overlapping horizontal counters yielding seven bins. Thus each grid element had the dimensions 1.1" by 0.85" and the typical angular acceptance in the horizontal direction was about 2.9°.

The two radiation lengths of lead converted about 80% of the incident photons; the biases on the hodoscope counters were set so that each counter was 100% efficient for minimum ionizing particles. This assured us that all converting photons would be detected.

The lead-lucite Cerenkov shower counter consisted of six lucite plates attached to one lucite light pipe, with five radiation lengths of lead between the plates. A 5" RCA 7046 phototube collected the light.

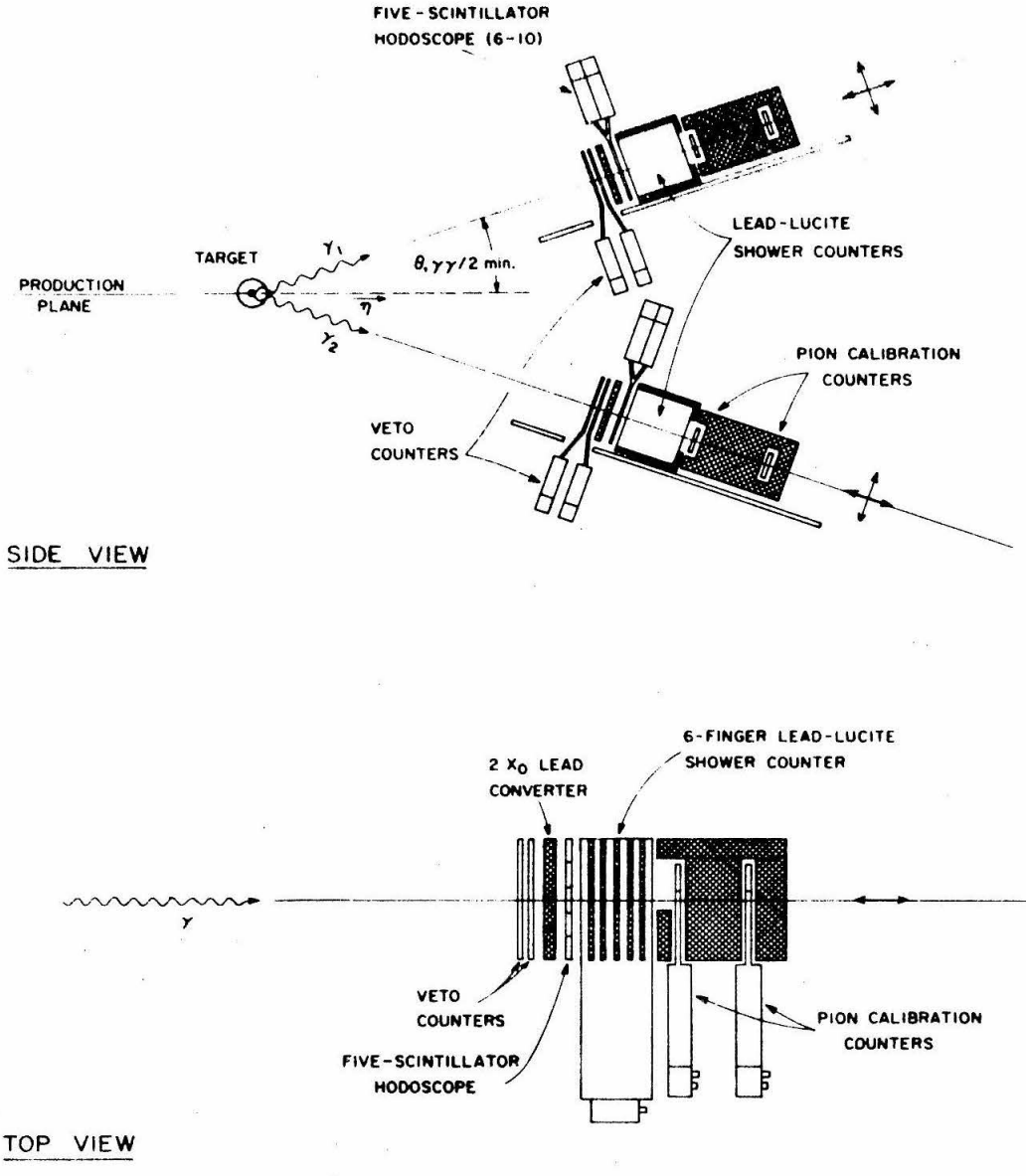

Figure 6.2 The photon detection system (horizontal hodoscopes not shown).

The light intensity was roughly proportional to the energy of the photon (for normal incidence near the center of the counter), with a Gaussian sigma of 10% at 1000 MeV and depending upon energy as $E^{-\frac{1}{2}}$. As explained earlier, foreground events had a very different pulse height spectrum from background events and by setting aminimum value upon the photon pulse heights, we were able to further reduce background contamination. As a result, some small number of eta events were lost, but the background events were depleted much more. From the results of a lengthy investigation by L. S. Rochester on the effects of non-normal incidence and on edge effects with the very same shower counters for his cross-section experiment,[13] we find that the pulse height spectrum for mono-energetic photons begins to collapse very strongly for photons showering within one centimeter of the edge of the 6" x 10" aperture of the shower counter, so that by applying a minimum pulse height to accept an event, we are effectively throwing out η events whose photons (one or both) shower in this region.

The two shower counters were calibrated with monoenergetic electrons of normal incidence. In addition, a $\beta = 1$ peak was obtained by removing the lead between the lucite plates and passing 600 MeV electrons through the counter. Our results were consistent with those of L. S. Rochester.[13]

It was important to monitor the performance of the shower-counters during the running of the experiment and for this purpose, as in our previous experiments, two small scintillation counters with six inches of lead between them were placed behind each shower counter. A trigger

of these two counters in coincidence provided a source of non-showering particles (fast pions and muons) of $\beta \geq 0.96$. Periodically during the experiment, the gains of the shower counters were checked with this source and the biases on the counters were set with respect to the resulting minimum ionizing distributions. The biases were set in such a way as to minimize false triggers from $\beta = 1$ particles or low energy photons from background processes while not at the same time cutting significantly into the spectrum of true η events. We estimate that with our bias settings we lost only a small percentage of the true events for Set I, whereas for Set II, the number was more like 10%. This situation could not be tolerated in a cross-section measurement; for our purposes, these settings gave us, especially for Set II, a much richer sample of η events on the film with the slight increase in running time (to obtain a given number of events) outweighed by the decrease in scanning time.

4. Proton Telescope

A. Apparatus

The proton telescope consisted of three scintillation counters and three spark chambers, as shown in figure 6.3. It is essentially the same as that used in previous experiments in our group. The first scintillator was 6" x 10" while the other two measured 17.5" x 17.5". All were ¼" thick. The counters were arranged such that a proton traveling in a straight line from any portion of the target and passing through the third proton scintillation counter would automatically have passed through the other two scintillators. The biases on the proton

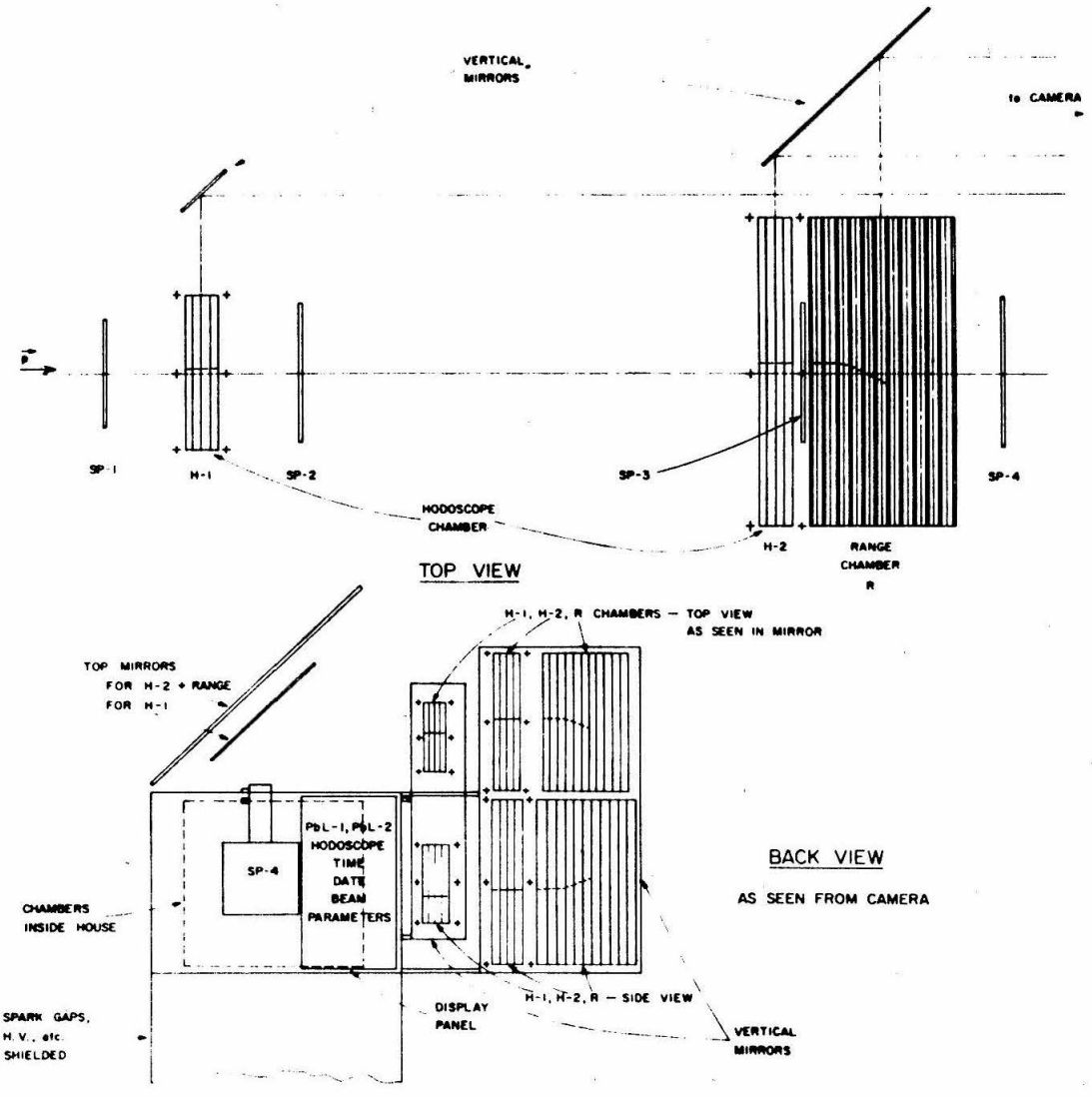

Figure 6.3 The proton detection system.

counters were set in such a way as to exclude minimums without cutting into the slower and therefore more heavily ionizing protons. A pulse-height spectrum for protons for any one of the scintillation counters was obtained by use of an additional 1" scintillator. With a large pulse height requirement upon this counter in coincidence with the scintillator in question and with enough carbon between the two scintillators to stop a 250 MeV proton (≃ 30 cm), we were able to easily distinguish between a proton and a minimum ionizing spectrum. In addition, the maximum of the proton spectrum always occurred at exactly the place, relative to the minimum peak, predicted by energy loss of particles in matter tables.

The two thin foil chambers between the proton scintillation counters each contained four gaps separated by 0.001" aluminum foil. The active area of the first was 8" x 10" and of the second, 17.5" x 17.5". The range-scattering chamber was modular--two gap sparking modules alternating with carbon modules. These have been described before,[19] and are shown in detail in figure 6.4. The carbon plates were 1 cm and 1.5 cm thick; an attempt was made to arrange these sizes in the range-scattering chamber in such a way as to maximize resolution, for each setting, in the vertex of the scatter and in the proton stopping point. However, it was found that our resolution was very insensitive to any such arrangement.

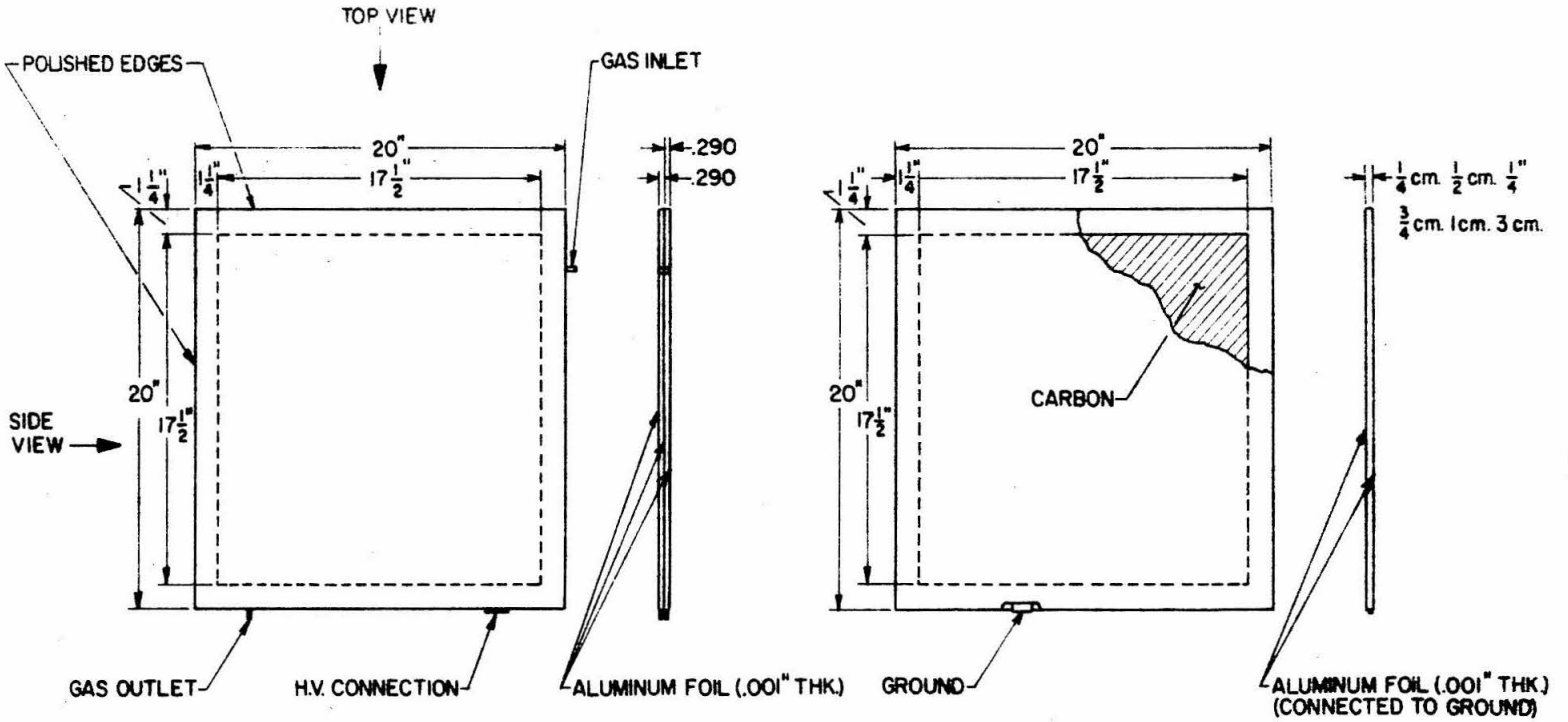

Figure 6.4 Details of chamber module construction.

B. Optics and Fiducials

The lenses and mirrors used to send two views 90° apart of all three chambers to the camera are shown in figure 6.3 as well as in figure 6.5. Lenses were required to see into the spark gaps of the range chamber because of its size; they were plano-convex, each with a focal length of 19' 2". The effect of distortions was checked after our system was aligned by photographing a specially made grid at several positions in the region of the range chamber. Both horizontal and vertical distortions were checked for and found to be negligible.

The fiducials, appearing as plus signs in figure 6.5, were machined onto lucite strips which were end-lighted. The strips were mounted independently of the spark chambers. The distance of the fiducial frame from the origin was known to about 1 mm while the inter-fiducial distances were measured to an accuracy of about 0.1 mm.

5. Electronics

In figure 6.6 and figure 6.7 we see the main features of our logic and readout systems. In both figures, SP refers to counters in the proton telescope and PbL to the lead-lucite shower counters. For a discussion of the logical requirements for an event trigger, see Section II. By requiring a veto signal to be a coincidence between one veto counter and the shower counter on the opposite side, we were able to effectively reduce our veto dead-time. Our coincidence delay curve widths of 20 ns resulted in a negligible loss of events.

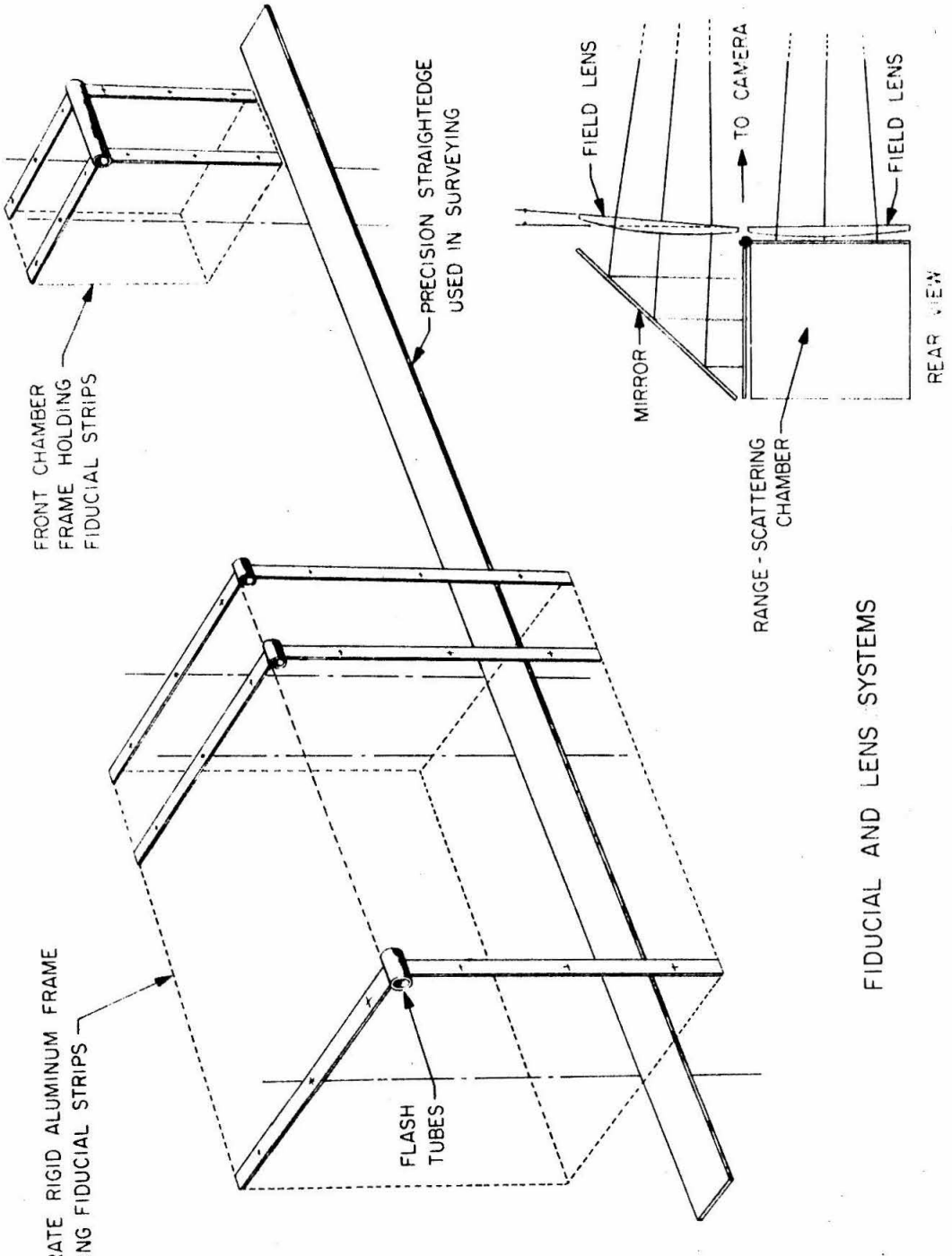

FIDUCIAL AND LENS SYSTEMS

Figure 6.5

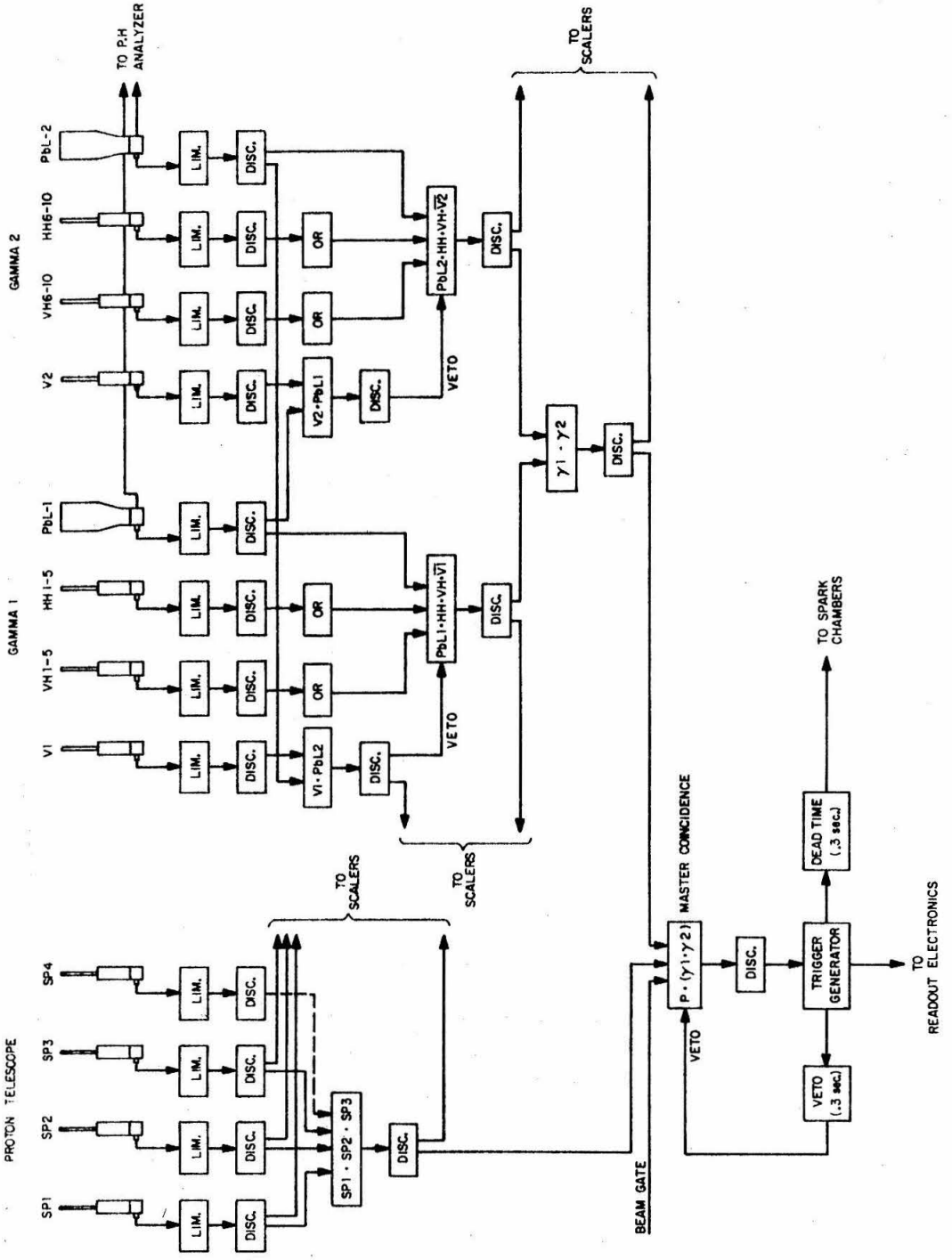

Figure 6.6 Fast logic for eta trigger.

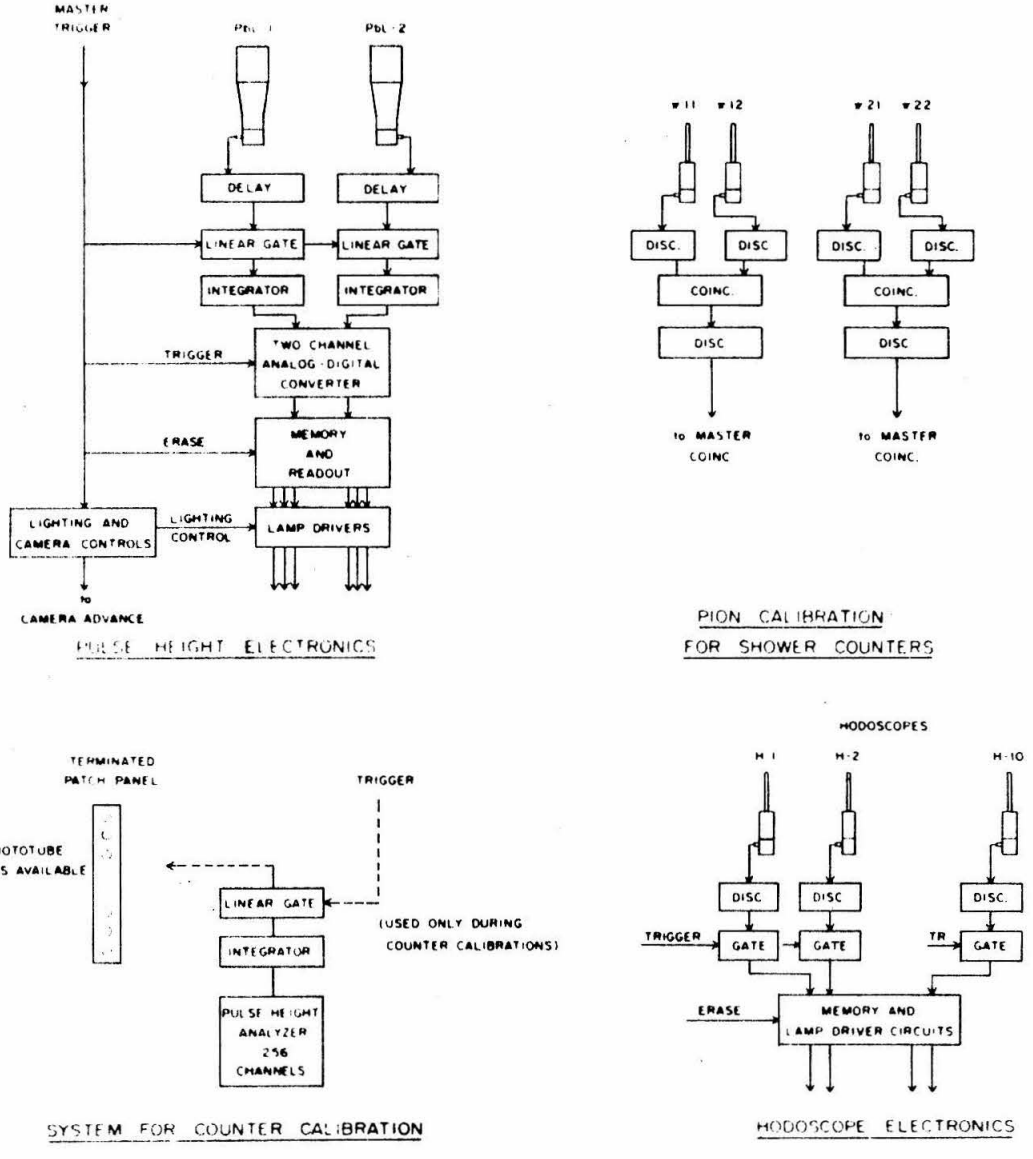

Figure 6.7 Readout and calibration systems.

6. Scanning and Measuring Criteria

Every one of the 280,000 pictures was scanned twice (each roll of film being looked at by two individuals) by trained scanners, many of whom had had previous experience working on a polarization experiment. To be considered a possible scatter, the proton track had to fulfill the following criteria:

1) The event must have a clear scatter of at least 3° in either of the two views of the range-scattering chamber.

2) The track length after the scatter must be long enough to measure well (usually three sparking modules).

3) The event must have only one scatter.

4) The event must be correlated in all chambers.

Both lists of scatters, each generated by a different scanner, were looked at by a third scanner. The third scanner or verifier was one of two individuals for the entire experiment, the two most experienced scanners of the group. The verifier was the one who decided upon any events in contention. In practice, only events with scatters of 4° or more were used in the final analysis. Out of a sample of 680 such events, the scanning efficiency of the first group of scanners was 97.3% while that of the second group was 95.3%.

7. Events Leaving the Chamber; ϕ Resolution

A matter of importance in the present experiment is a consideration of events which may leave the scattering chamber after scattering. These must be thrown out since their range after scattering is uncertain and

necessary in the present experiment. The position of the last spark on each proton track was constructed and if the event could have traversed one more module without detection, the event was discarded.

Events which do not leave the chamber must also be looked at carefully to see that if they had scattered "the other way", they could have been detected. For an example, we consider the case where the scatter takes place in the plane of the reaction and we take this reaction plane to be parallel to the horizontal plane of the scattering chamber (which it is on the average). The proton polarization perpendicular to this plane is related to the left-right scattering asymmetry in this plane; the event shown at the top of figure 6.8 clearly cannot be used in a sample of events (scattering in the reaction plane) to determine the left-right scattering asymmetry as it could not have been fully detected had it scattered in the other direction.

At the bottom of figure 6.8 we show a way of representing an arbitrary scatter. The z-axis goes into the paper with the x-z plane representing the reaction plane. The solid line represents the proton after the scatter (the initial proton direction being along the z-axis) with ϕ being defined as indicated. The dotted lines represent scatters with related ϕ's as indicated.

From figure 6.8, we see that if we are interested in polarization perpendicular to the reaction plane, arising from an asymmetry <u>in</u> the reaction plane, the indicated scatter may be used in the likelihood analysis <u>without</u> modification for the following two cases: (we assume the scatter itself does not leave the chamber) (1) if the related

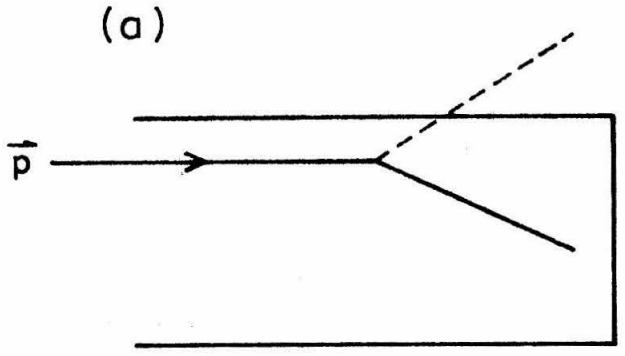

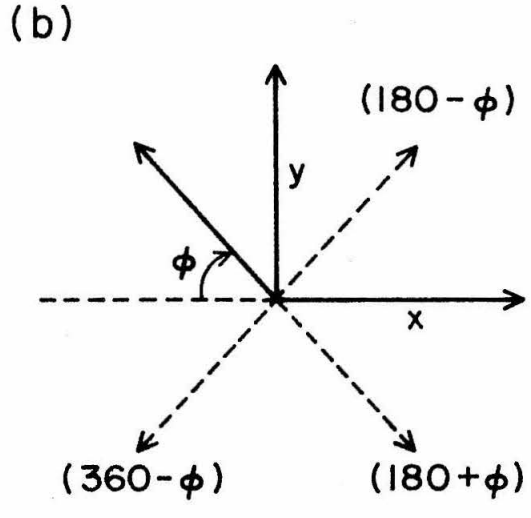

Figure 6.8 (a) Diagram of event not used in a likelihood analysis;

(b) representation of the ϕ in a p-C scatter, and of related scatters.

scatter at $\phi + 180^{\circ}$ does not leave the chamber; (2) if the related scatter at $\phi + 180^{\circ}$ does leave the chamber, the one at $180^{\circ} - \phi$ does not leave the chamber and the one at $360^{\circ} - \phi$ does leave the chamber; (this latter case is as though we are only sensitive to a ϕ region of π rather than 2π radians). Similar requirements can be stated for a determination of the polarization in the reaction plane.

Only 5% of our events failed to fall into one of these categories and these were not analyzed although a procedure for treating these is described in Appendix VI-10F.

As a check, the events were analyzed separately depending upon in which side of the chamber they occurred and the results were consistent (for both settings).

All events upon the final list (from the verifier) were measured as possible candidates for the reaction and a large sample of the events were measured and analyzed twice to give us an idea of how measuring errors would affect calculated quantities. The only quantity to vary significantly from measure to measure was the calculated ϕ of the p-C scatter, figure 6.8. The discrepancy varied depending upon the theta of the scatter, but on the average for the events used in the analysis, this discrepancy was about 8°. If we consider this a reflection of our resolution in ϕ, then our results must be modified slightly; this because the observed cosine ϕ will always be somewhat smaller than its actual value. The entire effect, however, is less than 1%. See reference 21.

8. Analyzing Power

The analyzing power of an element can be defined very simply as the asymmetry induced in the scattering of 100% polarized protons. Of course the analyzing power is a function of proton energy, the angle of the scatter, as well as the inelasticity of the scatter. The experimental method of double scattering of unpolarized protons to obtain the magnitude of the asymmetry[22] and that of slowing down the protons after the first scatter to less than 10 MeV and observing their asymmetry in scattering off of He_4 (whose analyzing power is calculable) to obtain its sign are well known.

A program written by W. A. McNeely[14] to interpolate between all the known p-C analyzing power data was used with a modification described in Section III to account for our lack of knowledge of the inelasticity of each p-C scatter.

In figure 6.9 we see a two dimensional representation of the elastic proton-Carbon analyzing power as fit by W. A. McNeely. As was mentioned previously, the analyzing power for the present experiment, when our lack of knowledge of the p-C inelasticity was accounted for, was, for a typical bin of events, about 20% less than the value calculated using the values in figure 6.9. Figure 6.10 shows the values of the analyzing power, when averaged over inelasticities, actually used in the present experiment.

ANALYZING POWER

THETA \ TP	95.0	115.0	135.0	145.0	155.0	170.0	180.0	200.0	220.0	255.0	289.0
3	0.0	0.0	0.0	0.0	0.0	0.151	0.350	0.286	0.214	0.068	0.0
4	0.078	0.118	0.214	0.307	0.367	0.395	0.374	0.359	0.330	0.244	0.123
5	0.214	0.296	0.358	0.384	0.401	0.408	0.402	0.426	0.430	0.389	0.296
6	0.222	0.315	0.384	0.410	0.428	0.439	0.435	0.486	0.514	0.504	0.427
7	0.214	0.305	0.384	0.421	0.449	0.471	0.474	0.539	0.578	0.583	0.512
8	0.214	0.307	0.390	0.431	0.463	0.496	0.509	0.578	0.621	0.631	0.566
9	0.214	0.310	0.400	0.447	0.486	0.525	0.540	0.624	0.676	0.688	0.608
10	0.205	0.321	0.425	0.478	0.518	0.555	0.565	0.658	0.716	0.728	0.637
11	0.205	0.317	0.435	0.508	0.560	0.596	0.594	0.698	0.760	0.772	0.666
12	0.215	0.333	0.455	0.527	0.580	0.622	0.626	0.743	0.812	0.815	0.679
13	0.227	0.348	0.479	0.558	0.619	0.675	0.689	0.798	0.856	0.838	0.676
14	0.240	0.363	0.507	0.599	0.672	0.741	0.761	0.851	0.892	0.847	0.665
15	0.255	0.379	0.538	0.649	0.731	0.798	0.806	0.887	0.918	0.856	0.654
16	0.285	0.401	0.572	0.704	0.797	0.860	0.852	0.917	0.933	0.840	0.607
17	0.314	0.435	0.610	0.745	0.839	0.904	0.896	0.933	0.923	0.791	0.528
18	0.344	0.474	0.651	0.782	0.875	0.938	0.931	0.931	0.890	0.719	0.437
19	0.373	0.516	0.695	0.822	0.909	0.969	0.961	0.908	0.834	0.651	0.416
20	0.401	0.562	0.743	0.863	0.944	0.991	0.972	0.872	0.768	0.578	0.387
21	0.429	0.605	0.786	0.904	0.972	0.978	0.919	0.782	0.660	0.492	0.351
22	0.458	0.648	0.813	0.913	0.952	0.893	0.777	0.629	0.510	0.371	0.321
23	0.486	0.691	0.823	0.882	0.881	0.765	0.613	0.458	0.348	0.262	0.307
24	0.514	0.734	0.817	0.811	0.761	0.603	0.443	0.313	0.229	0.189	0.289
25	0.542	0.778	0.795	0.702	0.591	0.390	0.232	0.159	0.120	0.134	0.243
26	0.569	0.791	0.746	0.587	0.435	0.217	0.080	0.103	0.060	0.060	0.177
27	0.564	0.775	0.676	0.448	0.265	0.076	0.006	0.080	0.008	0.000	0.061
28	0.551	0.726	0.588	0.329	0.135	0.000	0.000	0.000	0.000	0.000	0.004
29	0.527	0.632	0.490	0.272	0.099	0.000	0.000	0.000	0.000	0.000	0.000
30	0.494	0.501	0.376	0.244	0.120	0.000	0.000	0.000	0.000	0.000	0.000

Figure 6.9 Elastic proton-carbon analyzing power as fit by W. A. McNeely.

ANALYZING POWER

THETA \ TP	95.0	115.0	135.0	145.0	155.0	170.0	180.0	200.0	220.0	255.0	289.0
3	0.0	0.0	0.0	0.0	0.0	0.144	0.338	0.281	0.214	0.070	0.0
4	0.068	0.100	0.186	0.272	0.331	0.367	0.353	0.343	0.320	0.244	0.128
5	0.187	0.254	0.311	0.341	0.361	0.383	0.380	0.404	0.409	0.377	0.294
6	0.197	0.276	0.344	0.375	0.395	0.417	0.414	0.463	0.490	0.484	0.416
7	0.196	0.277	0.350	0.387	0.416	0.447	0.450	0.510	0.546	0.550	0.486
8	0.197	0.281	0.359	0.398	0.432	0.469	0.481	0.543	0.580	0.584	0.523
9	0.198	0.286	0.370	0.413	0.452	0.492	0.504	0.576	0.618	0.617	0.540
10	0.190	0.297	0.392	0.440	0.481	0.517	0.524	0.602	0.646	0.643	0.555
11	0.190	0.294	0.401	0.465	0.513	0.544	0.540	0.621	0.663	0.650	0.548
12	0.198	0.308	0.416	0.477	0.524	0.558	0.558	0.645	0.687	0.662	0.538
13	0.209	0.321	0.434	0.497	0.546	0.587	0.594	0.666	0.693	0.648	0.512
14	0.220	0.334	0.453	0.525	0.579	0.627	0.638	0.692	0.706	0.641	0.494
15	0.230	0.345	0.466	0.547	0.605	0.649	0.651	0.695	0.700	0.626	0.475
16	0.253	0.361	0.482	0.570	0.627	0.661	0.650	0.675	0.665	0.574	0.423
17	0.274	0.383	0.491	0.570	0.620	0.651	0.640	0.644	0.621	0.521	0.375
18	0.290	0.406	0.499	0.564	0.607	0.632	0.621	0.607	0.573	0.468	0.333
19	0.307	0.430	0.497	0.547	0.579	0.599	0.589	0.558	0.519	0.422	0.313
20	0.323	0.452	0.502	0.539	0.564	0.579	0.568	0.527	0.486	0.397	0.300
21	0.329	0.459	0.494	0.518	0.544	0.557	0.542	0.506	0.469	0.386	0.297
22	0.337	0.471	0.454	0.470	0.485	0.487	0.465	0.437	0.409	0.342	0.272
23	0.341	0.480	0.433	0.448	0.470	0.487	0.471	0.456	0.437	0.377	0.308
24	0.341	0.490	0.428	0.419	0.427	0.438	0.422	0.408	0.388	0.330	0.270
25	0.342	0.489	0.420	0.395	0.397	0.410	0.396	0.390	0.373	0.316	0.257
26	0.319	0.460	0.407	0.378	0.381	0.391	0.376	0.378	0.060	0.050	0.245
27	0.302	0.425	0.390	0.357	0.360	0.367	0.354	0.080	0.008	0.000	0.227
28	0.290	0.395	0.374	0.343	0.347	0.352	0.340	0.000	0.000	0.000	0.214
29	0.282	0.372	0.356	0.338	0.346	0.343	0.325	0.000	0.000	0.000	0.201
30	0.277	0.329	0.330	0.331	0.346	0.321	0.298	0.000	0.000	0.000	0.000

Figure 6.10 Proton-carbon analyzing power values used in the present experiment (inelasticities averaged over).

9. Conservation of Parity

We first consider the process p-C → p-C. Carbon is a spin zero nucleus; therefore the most general amplitude for this process, consistent with parity conservation, is of the form

$$\langle \psi_f \, | f + g \vec{\sigma} \cdot \hat{n} | \, \psi_i \rangle$$

where ψ_i and ψ_f are the initial and final proton spinors, and $\hat{n}$ is a unit vector normal to the scattering plane. The quantities f and g are functions of energy and angle, but not of spin.

The differential cross-section for this process is

$$\frac{d\sigma}{d\Omega} = \langle \psi_i \, | (f^* + g^* \vec{\sigma} \cdot \hat{n}) \, (f + g \vec{\sigma} \cdot \hat{n}) | \, \psi_i \rangle$$

$$= |f|^2 + |g|^2 + 2 \, \mathrm{Re} \, f^* \, g \, \langle \psi_i | \vec{\sigma} \cdot \hat{n} | \, \psi_i \rangle$$

$$= |f|^2 + |g|^2 + 2 \, \mathrm{Re} \, f^* \, g \, (\vec{P}_{in} \cdot \hat{n})$$

where $\vec{P}_{in}$ is the incoming polarization.

If we make the identification

$$A = \frac{2 \, \mathrm{Re} \, f^* \, g}{|f|^2 + |g|^2} \, ,$$

we can write

$$\frac{d\sigma}{d\Omega} \alpha \; 1 + A(\vec{P}_{in} \cdot \hat{n}).$$

This is the origin of the expressions used in the likelihood function.

Let us now calculate the polarization, $P_{out} = \langle \psi_f \, \vec{\sigma} \, \psi_f \rangle$, of the

final state proton for the process p-C → p-C.

$$\frac{d\sigma}{d\Omega}\vec{P}_{out} = \langle\psi_i | (f^* + g^*\vec{\sigma}\cdot\hat{n})\vec{\sigma}(f + g\vec{\sigma}\cdot\hat{n})|\psi_i\rangle .$$

When the Pauli spin algebra is completed, the result is

$$\frac{d\sigma}{d\Omega}\vec{P}_{out} = (|f|^2 - |g|^2)\vec{P}_{in} + 2|g|^2(\vec{P}_{in}\cdot\hat{n})\hat{n} - 2\,\mathrm{Im}\,(f^*g)\hat{n}\times\vec{P}_{in}$$
$$+ 2\,\mathrm{Re}\,f^*g\,\hat{n} .$$

We note in particular that if $\vec{P}_{in} = 0$, then $\vec{P}_{out}$ is only in the direction of $\hat{n}$, the normal to the reaction plane.

We will state here that the result is the same for two-body photoproduction: if the initial protons and photons are unpolarized, then the final state polarization is in the direction of the normal to the reaction plane. This follows from writing down the most general parity conserving amplitude for photoproduction (this time including the photon polarization vector, $\vec{\varepsilon}$), and calculating the final state polarization for an unpolarized initial state.

In the case of a background process with more than a two-body final state, such as $\gamma p \to p\pi^o\pi^o$, the extra degree of freedom in the final state allows parity conserving interaction terms which yield a polarization in a direction other than $\vec{k}\times\vec{p}$, (for instance the term $\vec{\sigma}\cdot(\vec{k}\times\vec{p}_{\pi^o})$).

10. The Maximum Likelihood Method[1]

A. The First Moment

If a beam of N protons with polarization P in the z direction is incident on the origin along the y axis, the number of events scattering at angle ϕ is given by the expression

$$N(\phi)\, d\phi = N \frac{(1 + A\ P \cos\phi)}{2\pi} d\phi \qquad 10.1$$

where A is the analyzing power of the scatter (assumed for now to be constant for all N scatters) and where all N events do scatter. The larger N, the more correct will be this expression. We see that the average value of the cosine of the angle is given by

$$\overline{\cos\phi} = \frac{1}{N} \int_0^{2\pi} N(\phi) \cos\phi\, d\phi = \frac{A\ P}{2}$$

so that

$$P = \frac{2\ \overline{\cos\phi}}{A} \qquad 10.2$$

If however, all scatters do not have the same analyzing power, but instead there are N_i events with analyzing power A_i, then

$$N(\phi)\, d\phi = \sum_i \frac{N_i (1 + A_i\ P \cos\phi)}{2\pi} d\phi \qquad 10.3$$

and

$$\overline{\cos\phi} = \frac{P}{2} \sum_i \frac{N_i\ A_i}{N}$$

---

(1) The material in this section is treated much more fully in ref. 21.

so that

$$P = \frac{2\ \overline{\cos\phi}}{\bar{A}}$$

where $\bar{A}$ is the average analyzing power. For the 24 bins of events in the present experiment for which polarization values are reported (foreground, background, in the plane and out of the plane), the above simple minded determination of the polarization agreed in all cases with the value obtained from the maximum likelihood method to within about 30% of an error bar.

We would like to calculate the statistical error in P from the above simple-minded expression. For this, we use the central limit theorem: the standard deviation in the average of N measurements of a quantity (in this case $\cos\phi$) is equal to the square root of the second moment about the mean of the quantity, divided by the square root of N. For A = 1, the average value of $\cos\phi$ is just P/2 so that we have

$$\overline{(\cos\phi - P/2)^2} = \frac{1}{N} \int N(\phi)\ (\cos\phi - P/2)^2\ d\phi$$

$$= \frac{1}{2\pi} \int_0^{2\pi} (1 + P\cos\phi)\ (\cos^2\phi - P\cos\phi + \frac{P^2}{4})d\phi = \frac{1}{2} - \frac{P^2}{4}$$

and therefore

$$(\Delta\cos\phi)^2 = (\frac{1}{2} - \frac{P^2}{4})/N$$

giving us the expression for ΔP:

$$\Delta P = \sqrt{\frac{2}{N}}\ \sqrt{1 - P^2/2} = \sqrt{\frac{2}{N}}\left[\ 1 - \frac{P^2}{4} - \frac{P^4}{16} - \ .\ .\ .\right] \quad 10.4$$

Again, if our distribution were as in expression 9.3 we would get

$$\Delta P = \frac{1}{\bar{A}} \sqrt{\frac{2}{N}} \sqrt{1 - \frac{\bar{A}^2 P^2}{2}}$$

In the present experiment, $\bar{A}P$ was always less than .7 so that the expression

$$\Delta P = \frac{1}{\bar{A}} \sqrt{\frac{2}{N}}$$

is accurate and reproduces our errors as calculated by the maximum likelihood method.

B. The Likelihood Function

As pointed out in the beginning of this section, a proton scattering with analyzing power A has a probability proportional to

$$\frac{1 + A\ P\ \cos\phi}{2\pi}$$

of scattering at the azimuthal angle ϕ where again we are assuming P is in the z direction. A depends upon the polar scattering angle (not ϕ) as well as the proton energy and the inelasticity of the scatter.

If we ask now, what is the probability that N protons will scatter with angles ϕ_i where the analyzing powers of the scatters are A_i, the answer is

$$P(\phi_1, \phi_2 \cdots \phi_N) = \prod_{i=1}^{N} \frac{(1 + A_i\ P\ \cos\phi_i)}{2\pi} ,$$

simply the product of the individual probabilities. The above expression can be looked upon as the probability of generating an experiment

with the given phi distribution. We note that

$$\int_0^{2\pi} \cdots \int_0^{2\pi} \int_0^{2\pi} P(\phi_1, \phi_2 \ldots \phi_n)\, d\phi_1\, d\phi_2 \ldots d\phi_n = 1 ,$$

i.e., the sum of the probabilities of every experiment is one.

This same expression, however, can be looked upon as a function of P:

$$L(P) = \prod_{i=1}^{N} \frac{1 + A_i P \cos\phi_i}{2\pi}$$

In words, it is the probability of generating a given experiment $(\phi_1, \phi_2 \ldots \phi_n)$ as a function of polarization P. Thus, for a given experiment, the value of P for which L(P) is maximum is the most likely value of the polarization. As such, L(P) is called the likelihood function.

In practice, this was the method by which the polarization values perpendicular to the reaction plane reported in the present experiment were obtained. In all cases, L(P) was relatively narrow and was very nearly a Gaussian through the whole range of P, from -1 to 1.

For a determination of polarization values <u>in</u> the reaction, the following function was maximized:

$$L(P_{\parallel}) = \prod_{i=1}^{N} \frac{1 + A_i P_{\parallel} \sin\phi_i}{2\pi} \qquad 10.5$$

If one allows for polarization both perpendicular and parallel to the reaction plane, the expression analagous to 10.1 is

$$N(\phi)\, d\phi = \frac{N(1 + A\, P_{\perp} \cos\phi + A\, P_{\parallel} \sin\phi)}{2\pi}\, d\phi$$

so that the function to maximize becomes

$$L(P_{\perp}, P_{\parallel}) = \prod_{i=1}^{N} \frac{(1 + A_i\, P_{\perp} \cos\phi_i + A_i\, P_{\parallel} \sin\phi_i)}{2\pi}$$

However, it can be shown[21] that the use of expression 10.5 instead of the above expression for determination of $P_{\parallel}$ yields exactly the same result; the only difference being an insignificant (less than 3% for the present experiment) change in the error bars (which are the Gaussian widths of the likelihood functions).

C. The Analytic Function $L(P, P_o)$

We would like to answer the following question: if a beam of N protons of polarization P_o scatter with analyzing power 1, what does the likelihood function for the resulting ϕ distribution look like?

We first note the following:

$$L(P) = \prod_{i=1}^{N} \frac{1 + P \cos\phi_i}{2\pi}$$

$$\ln L(P) = \sum_{i=1}^{N} \ln \left(\frac{1 + P \cos\phi_i}{2\pi}\right) \qquad 10.6$$

For a particular <u>smooth</u> distribution of events $N(\phi)$, the above expression becomes:

$$\ln L(P) = \int_0^{2\pi} N(\phi) \ln \frac{1 + P \cos\phi}{2\pi}\, d\phi$$

In particular, for N scatters with proton polarization P_o,

$$N(\phi) = N \frac{1 + P_o \cos\phi}{2\pi}$$

so that we can define

$$\ln L(P, P_o) = N \int_0^{2\pi} \left(\frac{1 + P_o \cos\phi}{2\pi}\right) \ln \frac{1 + P \cos\phi}{2\pi} \, d\phi$$

to be the logarithm of the function we are interested in. In words, $L(P, P_o)$ is the likelihood function for an experiment whose ϕ distribution is that arising from an ideal scattering experiment done with N protons of polarization P_o.

The above integral can be done exactly yielding:

$$\ln L(P, P_o) = N \left[\ln \left(\frac{1 + \sqrt{1 - P^2}}{2}\right) + P_o \left(\frac{1 - \sqrt{1 - P^2}}{P}\right)\right]$$

The above expression yields a limiting analytic form for the likelihood function. We expect the function $L(P, P_o)$ to be nearly Gaussian and centered at P_o.

Writing

$$\ln L(P, P_o) = N \sum_{n=2}^{\infty} (P - P_o)^n f_n(P_o),$$

it can be shown that

$$f_n(P_o) = \frac{n - 1}{n!} \left(-\frac{d}{dP_o}\right)^{n-2} \left| \frac{1}{P_o^2} \left(\frac{1}{\sqrt{1 - P_o^2}} - 1\right) \right|$$

so that we can write:

$$f_2(P_o) = \frac{1}{2}\left[\frac{1}{2} + \frac{3P_o^2}{8} + \frac{P_o^4}{16} + \ldots\right]$$

From which we can derive an expression for σ, assuming $L(P, P_o)$ to have the form

$$L(P, P_o) \propto e^{-(P-P_o)^2/2\sigma^2}.$$

We get

$$\sigma = \sqrt{\frac{2}{N}}\left[1 - 3P_o^2/4 - P_o^4/16 - \ldots\right].$$

Comparing with 10.4 we see the size of the advantage of the likelihood approach.

D. Higher Moments

It can be shown in another way that the method of maximum likelihood is better, although not by much, than the method of simply equating P to twice the average value of the cosine of phi. Briefly, taking the derivative of 10.6 with respect to P and setting the result to zero, the equation which the most likely value of P must satisfy is

$$\sum_{i=1}^{N} \frac{\cos\phi_i}{1 + P\cos\phi_i} = 0$$

where we have taken A = 1 for simplicity. Expanding, we have

$$\sum_{i=1}^{N} \cos\phi_i \left(1 - P\cos\phi_i + P^2\cos^2\phi_i - P^3\cos^3\phi_i + \ldots\right) = 0$$

This is equivalent to the expression

$$\overline{\cos\phi} - P\,\overline{\cos^2\phi} + P^2\,\overline{\cos^3\phi} - P^3\,\overline{\cos^4\phi} + \ldots = 0$$

where the "bars" mean average values. Keeping only the first two terms, we obtain

$$P = \frac{\overline{\cos\phi}}{\overline{\cos^2\phi}} \qquad 10.7$$

which is equivalent to expression 10.2 when we set A=1 and $\overline{\cos^2\phi} = \frac{1}{2}$ as it is for a large number of events.

We also note that equation 10.7 is satisfied exactly by $P = 2\,\overline{\cos\phi}$ if our distribution of events is of the form $N(\phi) = \frac{N(1 + P\cos\phi)}{2\pi}$. We recall that expression 10.2 for P was derived by considering what the average value of $\cos\phi$ was for our perfect distribution in terms of P. Equivalently, we could have calculated the average of $\cos^3\phi$:

$$\overline{\cos^3\phi} = \frac{1}{N}\int_0^{2\pi} \frac{N(1 + P\cos\phi)}{2\pi}\cos^3\phi\, d\phi = \frac{3}{8}P$$

so that we have $P = \frac{8}{3}\,\overline{\cos^3\phi}$. If however, we calculate our statistical error in the above determination of P, in the manner done for the expression involving $\cos\phi$, we find the result less certain. We see that we could write down an infinite number of equations involving the moments of powers of $\cos\phi$ which P should satisfy; they are of the form

$$P = C_n\,\overline{\cos^{2n+1}\phi},$$

where

$$C_n = \frac{1}{2\pi} \int_0^{2\pi} \cos^{2n}\phi \, d\phi$$

$$= \frac{1}{\sqrt{\pi}} \frac{\Gamma\left(\frac{2n+1}{2}\right)}{\Gamma\ (n+1)}$$

The maximum likelihood method as exhibited in equation 10.7 is the one method which uses <u>all</u> of the above equations relating P to the moments of powers of cosine phi of the experimental distribution, each weighted with the proper significance. For a finite number of events, N, the higher the moment taken, the less significant is the resulting equation as we eventually begin to probe the experimental distribution for structure beyond the average spacing of the events. Since $\cos^n\phi$ contains terms up to $\cos n\phi$, its effective "wave length" is π/n so that, for a sample of N events, we expect equations involving moments of $\cos\phi$ beyond about $n = \frac{N}{2}$ to be totally without information.

E. The Magnitude of the Likelihood Function

We have spoken up to now only of the width of the likelihood function and of the value of P at which it is maximum. We will say something of the actual value of the function at its peak which does yield information not contained in the width. The function we have defined above as $L(P, P_o)$ when evaluated at $P = P_o$ is

$$L(P_o, P_o) = \exp\left[N \int_0^{2\pi} \frac{(1 + P_o \cos\phi)}{2\pi} \ln \frac{1 + P_o \cos\phi}{2\pi} \, d\phi \right] \quad 10.8$$

and this number represents the value the likelihood function takes at its peak for a perfect distribution of N scatters of polarization P_o.

The actual experimental distributions are not perfect so that it is useful to compare the height of the likelihood function for each experimental bin with that of the function had the distribution been perfect.

The generalization of 10.8 to the case when each event has a different analyzing power is given by the expression

$$\ln L_{exp}(P_o, P_o) = \sum_{i=1}^{N} \ln L(A_i P_o, A_i P_o).$$

From this expression and the definition of $L(P_o, P)$, we obtain the result

$$L_{exp}(P_o, P_o) = \prod_{i=1}^{N} \left(\frac{1 + \sqrt{1 - A_i^2 P_o^2}}{2}\right) e^{\sum_{i=1}^{N} (1 - \sqrt{1 - A_i^2 P_o^2})}$$

This number was calculated for each experimental bin after P_o was determined from the maximum likelihood method, and it was compared with the height of the likelihood function for that particular bin; it was found that in all cases, the numbers were indeed very close (never more than a 10% discrepancy). For further interpretation see reference 21 where it is shown that the height of the likelihood function contains the information in the value of χ^2 one would obtain by a least squares fit of experimental distribution in ϕ to the distribution in 10.3 (whereas the width of the likelihood function contains the information in the derivative of χ^2 with respect to P at P_o).

F. The Likelihood Function for a Limited Range of ϕ.

Finally, we wish to quote a result by which one can use events where only part of the 360° range of ϕ is available. We take the case where the experiment is sensitive to a region in ϕ between ϕ_1 and ϕ_2. In general, ϕ_1 and ϕ_2 are different for each scatter. For the above case, the angular distribution between ϕ_1 and ϕ_2 is now given by

$$N(\phi)\, d\phi = \frac{1 + P\cos\phi}{(\phi_2 - \phi_1) + P(\sin\phi_1 - \sin\phi_2)}\, d\phi$$

and the correct likelihood function becomes:

$$L(P) = \prod_{i=1}^{N} \frac{1 + P\cos\phi_i}{(\phi_{2_i} - \phi_{1i}) + P(\sin\phi_{1i} - \sin\phi_{2i})} \qquad 10.9$$

where we have explicitly shown the dependence of ϕ_2 and ϕ_1 on the event. The generalization to other than linear ranges in ϕ is obvious.

In practice, one could calculate ϕ_1 and ϕ_2 for each event which scattered near the edge of the chamber and then use the above form in the likelihood method. However, only some 5% of the events could not be treated by the criteria described in Section VI-7 and these were not analyzed. In reference 21, we discuss the determination of error from expression 10.9.

VII. REFERENCES

1. C. Y. Prescott (private communication).
2. E. Bloom, C. Heusch, C. Prescott, and L. Rochester, Phys. Rev. Letters 19, 671 (1967).
3. S. U. Cheng et al., to be published.
4. D. E. Lundquist et al., Phys. Rev. 168, 1527 (1968).
5. C. A. Heusch, C. Y. Prescott, and R. F. Dashen, Phys. Rev. Letters 17, 1019 (1966).
6. R. G. Moorhouse, Phys. Rev. Letters 16, 772 (1966).
7. C. A. Heusch and F. Ravndal, CALT-68-249; to be submitted to Physical Review.
8. L. D. Roper, Phys. Rev. Letters 12, 340 (1964); L. D. Roper, R. M. Wright, and B. T. Feld, Phys. Rev. 138, B190 (1965).
9. K. J. Foley et al., Phys. Rev. Letters 19, 397 (1967).
10. I. M. Blair et al., Phys. Rev. Letters 17, 789 (1966); E. Gellert et al., Phys. Rev. Letters 17, 884 (1966).
11. E. W. Anderson et al., Phys. Rev. Letters 16, 855 (1966); G. Bellettini et al., Phys. Letters 18, 167 1965).
12. W. A. McNeely et al.
13. E. D. Bloom, C. A. Heusch, C. Y. Prescott, and L. S. Rochester, Phys. Rev. Letters 21, 1100 (1968).
14. W. A. McNeely, CTSL Internal Report 30.
15. S. U. Cheng, experiment on recoil proton polarization in π^o photoproduction, to be published.

16. L. S. Rochester, Ph. D. Thesis, California Institute of Technology (1968).

17. C. Y. Prescott, Ph. D. Thesis, California Institute of Technology (1966).

18. Landau and Lifshitz, Quantum Mechanics, Non-Relativistic Theory (Addison-Wesley Publishing Company, Inc., 1958) p. 407.

19. Reference 17, for Hydrogen target; E. D. Bloom, Ph. D. Thesis, California Institute of Technology (1967), for chamber module construction.

20. See reference 16, and E. D. Bloom, Ph. D. Thesis, California Institute of Technology (1967).

21. B. D. Winstein, Features of the Maximum Likelihood Method in Application to Polarization Experiments, CALT Internal Report, in preparation.

22. L. Wolfenstein, Ann. Rev. Nuclear Sci. 6, 43 (8-11). (See M. J. Brinkworth and B. Rose, Nuovo Cimento, Volume III, Page 195 (1956) for the determination of the sign of the analyzing power.)

23. P.S.L. Booth et al., Daresbury Laboratory Preprint DNPL/P11(1969).

24. R.P. Bajpai and A. Donnachie, Nuclear Physics B12, 274-280 (1969).